The Plant Cell, Vol. 26: 3416–3434, August 2014, www.plantcell.org

Dynamics of Vacuoles and H$^+$-Pyrophosphatase Visualized by Monomeric Green Fluorescent Protein in *Arabidopsis*: Artifactual Bulbs and Native Intravacuolar Spherical Structures[W][OPEN]

Shoji Segami, Sachi Makino, Ai Miyake, Mariko Asaoka, and Masayoshi Maeshima[1]

Laboratory of Cell Dynamics, Graduate School of Bioagricultural Sciences, Nagoya University, Nagoya, Aichi 464-8601, Japan

We prepared *Arabidopsis thaliana* lines expressing a functional green fluorescent protein (GFP)-linked vacuolar H$^+$-pyrophosphatase (H$^+$-PPase) under the control of its own promoter to investigate morphological dynamics of vacuoles and tissue-specific expression of H$^+$-PPase. The lines obtained had spherical structures in vacuoles with strong fluorescence, which are referred to as bulbs. Quantitative analyses revealed that the occurrence of the bulbs correlated with the amount of GFP. Next, we prepared a construct of H$^+$-PPase linked with a nondimerizing GFP (mGFP); we detected no bulbs. These results indicate that the membranes adhere face-to-face by antiparallel dimerization of GFP, resulting in the formation of bulbs. In plants expressing H$^+$-PPase-mGFP, intravacuolar spherical structures with double membranes, which differed from bulbs in fluorescence intensity and intermembrane spacing, were still observed in peripheral endosperm, pistil epidermis and hypocotyls. Four-dimensional imaging revealed the dynamics of formation, transformation, and disappearance of intravacuolar spherical structures and transvacuolar strands in living cells. Visualization of H$^+$-PPase-mGFP revealed intensive accumulation of the enzyme, not only in dividing and elongating cells but also in mesophyll, phloem, and nectary cells, which may have high sugar content. Dynamic morphological changes including transformation of vacuolar structures between transvacuolar strands, intravacuolar sheet-like structures, and intravacuolar spherical structures were also revealed.

INTRODUCTION

H$^+$-translocating inorganic pyrophosphatase (H$^+$-PPase) catalyzes a coupled reaction of PPi hydrolysis and active proton transport across membranes. The biochemical properties, membrane topology, tertiary structure, gene expression profile, and physiological roles of H$^+$-PPase have been investigated in various organisms (reviewed in Maeshima, 2000; Gaxiola et al., 2007). In addition to acidification of vacuoles, H$^+$-PPases play a key role in the removal of excessive PPi from the cytoplasm (Ferjani et al., 2011). Two types of H$^+$-PPase, type I and type II, have been reported in various organisms (Drozdowicz and Rea, 2001). Type I H$^+$-PPases require a relatively high concentration of K$^+$ for enzymatic activity, but the type II enzymes do not. The type II H$^+$-PPases exist in the Golgi apparatus and related organelles, but in amounts <0.3% of those of the type I enzymes (Segami et al., 2010). Therefore, the type I enzyme has been predicted to be the key enzyme for vacuolar acidification as well as H$^+$-ATPase and PPi scavenger functions in plants.

The type I H$^+$-PPase is predominantly localized in the tonoplast (vacuolar membrane). However, localization of H$^+$-PPase has also been reported in the plasma membrane (PM) of the phloem companion cells, the cotyledons of pea (*Pisum sativum*) and the leaves and roots of *Arabidopsis thaliana* (Robinson et al., 1996; Langhans et al., 2001; Li et al., 2005; Paez-Valencia et al., 2011). The vacuole is a huge organelle with morphological and functional diversity in plant cells: examples include lytic vacuoles, protein storage vacuoles, pigment storage vacuoles, and the prevacuolar compartment (Martinoia et al., 2007). What organelles contain H$^+$-PPase? To understand the physiological role of H$^+$-PPase, knowing its localization in intracellular compartments, including vacuole-related organelles, is critical.

We examined the intracellular localization of H$^+$-PPase in *Arabidopsis* by expressing the functional enzyme tagged with green fluorescent protein (GFP). GFP, which is composed of 238 amino acid residues, is a sensitive reporter used to detect the intracellular localization of target proteins. The insertion or linkage of this relatively large molecule may cause dysfunction of enzymes and other proteins. Therefore, attention has been paid to avoiding artifacts from linkage with GFP. A problem in the visualization of vacuolar proteins is that GFP fluorescence is reduced under acidic conditions (Shaner et al., 2005). Moreover, a vacuolar papain-type cysteine protease degrades blue light-excited GFP in vacuoles (Tamura et al., 2003). To address these problems, we prepared a functional H$^+$-PPase in which GFP was inserted into an internal, unconserved cytoplasmic loop, and expressed the construct under the control of its own promoter.

In this study, GFP-linked H$^+$-PPase was detected in the membranes of the central vacuole in most cells and in the membranes of a small spherical structure called the bulb in

[1] Address correspondence to maeshima@agr.nagoya-u.ac.jp.
The author responsible for distribution of materials integral to the findings presented in this article in accordance with the policy described in the Instructions for Authors (www.plantcell.org) is: Masayoshi Maeshima (maeshima@agr.nagoya-u.ac.jp).
[W] Online version contains Web-only data.
[OPEN] Articles can be viewed online without a subscription.
www.plantcell.org/cgi/doi/10.1105/tpc.114.127571

immature cells. Bulbs were discovered as membranous structures in the central vacuoles when the aquaporin γ-TIP tagged with GFP was expressed in *Arabidopsis* (Saito et al., 2002). The word "bulb" has been used to describe fluorescent-labeled bulb-like structure seen in confocal images. Subsequently, bulbs were found in other plant tissues expressing GFP- and yellow fluorescent protein (YFP)-linked tonoplast proteins, such as aquaporins (α-TIP and δ-TIP), SNAREs (membrane proteins mediating vesicle fusion VAM3 and VTI11), and a phosphate transporter (PT1) (Saito et al., 2002, 2011a; Uemura et al., 2002; Escobar et al., 2003; Hicks et al., 2004; Reisen et al., 2005; Hunter et al., 2007; Beebo et al., 2009; Gattolin et al., 2009).

GFP has a tendency to form dimers (Yang et al., 1996; Zacharias et al., 2002). We thus carefully quantified the expression level of GFP-linked H+-PPase and its correlation with the appearance of bulbs and found that GFPs tagged to membrane intrinsic proteins, and not only H+-PPase, tend to adhere to the surface of neighboring vacuoles and to cause bulb formation. We prepared a monomer-type GFP by a single amino acid substitution and inserted it into the cytoplasmic loop of H+-PPase. There were no bulbs in the cells of plants expressing this construct. Here, we show evidence for the artifactual formation of bulbs and discuss a potential biochemical mechanism for this formation. These results will be useful in studies of cells using GFP.

We determined the intracellular localization of the enzyme at various growth stages by expressing monomeric GFP-linked H+-PPase with enzymatic function under the control of its own promoter. In these plants, intensive accumulation of H+-PPase was observed not only in dividing and elongating cells but also in mesophyll, phloem, and nectary cells. We discuss the high accumulation of the enzyme, taking into consideration the sugar content in those tissues. Furthermore, intravacuolar spherical structures (IVSPs) with double membranes, which were different from bulbs in fluorescence intensity and space between the membranes, were detected in various tissues, such as peripheral endosperm, pistil epidermis, and hypocotyl. An intravacuolar sheet-like structure and its transformation to the IVSP were also detected. We discuss these dynamic morphological changes in vacuoles and tonoplasts.

RESULTS

Construction of Functional GFP-Tagged H+-PPase

Both the N- and C-terminal regions of plant type I H+-PPase (hereafter referred to as H+-PPase, VHP1) face the vacuolar lumen (Figure 1A; Mimura et al., 2004; Lin et al., 2012). Generally, GFP localization to the vacuolar lumen is thought to be unfavorable (Tamura et al., 2003). Linkage of a large soluble protein like GFP may affect the translation or folding of membrane proteins in the endoplasmic reticulum (ER). Indeed, when we added GFP to the N or C terminus of H+-PPase, we did not detect fluorescence in the tonoplasts of over 50 individual transgenic plants of each construct, whereas ER-like structures with green fluorescence were detected in a few cases. We inferred that the addition of GFP to the N and C termini caused misfolding and mislocalization.

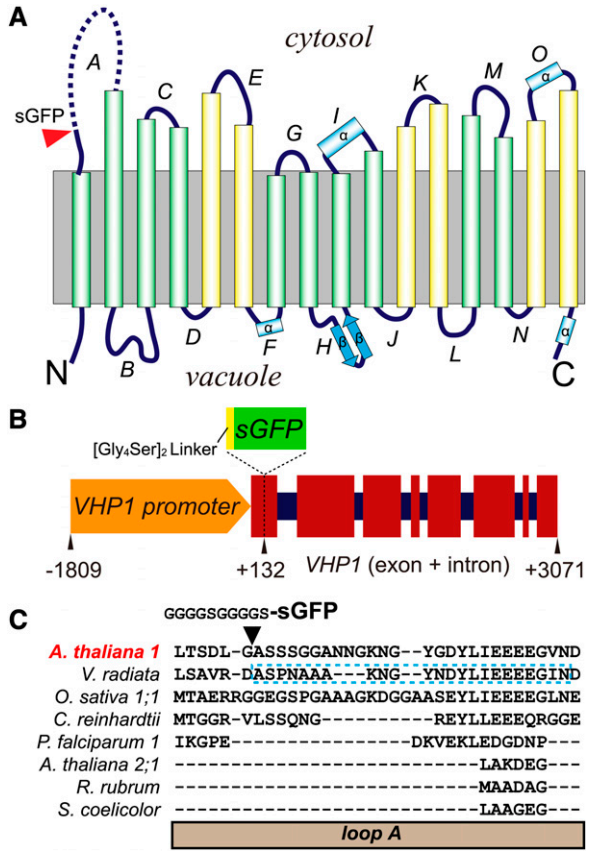

Figure 1. Construction of VHP1-GFP.

(A) Membrane topology of *Vigna radiata* H+-PPase (VHP1) on the basis of 3D structure (Lin et al., 2012). The insertion site of sGFP is marked by a red arrowhead. The undetermined region in loop A is shown by a broken line. The inner six transmembrane domains (TMs) and outer 10 TMs in the 3D structure of VHP1 are shown as green and yellow cylinders, respectively. Four α-helices and two β-strands of the TMs are marked as α and β, respectively.

(B) Schematic model of a VHP1-GFP construct. Exons and introns are respectively shown as wide red squares and narrow dark-blue squares. sGFP with a $[Gly_4Ser]_2$, a flexible linker, was inserted at position +132 of VHP1. Nucleotides −1809 to +3071 of the *VHP1* gene were subcloned from genomic DNA, and sGFP was inserted into the +132 bp position.

(C) Sequence alignment of loop A. The region of *V. radiata* VHP1 not determined by crystallography is marked by a blue-dotted-line box. The alignment was generated with the Mafft program (Katoh et al., 2002).

We next tried to insert GFP into the cytoplasmic loop of H+-PPase. To select a suitable site for GFP insertion, we compared the primary sequences of various H+-PPases. The unconserved region is not essential for enzyme function and is a good candidate for insertion of an exogenous sequence. Among the cytoplasmic loops, the first loop (loop *A*) is unique to each H+-PPase (Figure 1C). Furthermore, crystallography did not allow the structure of loop *A* of VrVHP1 to be determined, indicating relatively high flexibility (Lin et al., 2012). Thus, we inserted sGFP (Niwa et al., 1999) into loop *A* between Gly-44 and Ala-45 of the enzyme (hereafter referred to as VHP1-GFP) (Figure 1B). A 10-residue linker

($[Gly_4Ser]_2$) was added to the N terminus of sGFP to maintain structural flexibility between sGFP and H^+-PPase based on a previous report (Lewis et al., 2003).

This construct was used to transform the wild type (Columbia-0) and an H^+-PPase loss-of-function mutant *vhp1-1* (Ferjani et al., 2011) under the control of the *Arabidopsis VHP1* promoter. We obtained several transgenic lines that expressed VHP1-GFP at various levels in the background of the wild type (wA lines) and *vhp1-1* (vA lines). The PPi hydrolysis activity and the amount of H^+-PPase in crude membranes prepared from transgenic seedlings were increased compared with the wild type (Figures 2A to 2D). This indicates that VHP1-GFP expressed in plants shows normal PPi hydrolysis activity. In terms of proton pump function, a tonoplast enriched fraction prepared from suspension-cultured cells of the vA-12 line showed PPi dependent H^+-pumping activity (Supplemental Figure 1).

Cotyledons of *vhp1-1* mutant are rectangular, which is caused by the accumulation of PPi (Ferjani et al., 2011). This phenotypic property of *vhp1* was complemented by transformation with VHP1-GFP (Supplemental Figure 2), suggesting that the introduced VHP1-GFP is functional.

To examine the intracellular localization of VHP1-GFP, we centrifuged crude membranes from the VHP1-GFP/wild type plants on sucrose density gradients. The distribution of VHP1-GFP protein was the same as that of endogenous H^+-PPase and of tonoplast aquaporin γ-TIP (Figure 2E). Thus, we considered VHP1-GFP as a suitable reporter of the tonoplast with regards to enzyme activity, expression level, and intracellular localization.

VHP1-GFP Is Localized to the Central Vacuole and So-Called Bulbs

GFP-tagged H^+-PPase, VHP1-GFP, in wA and vA lines was detected in the tonoplast and also in spherical structures inside the tonoplast by confocal laser scanning microscopy (CLSM) (Figures 3A to 3C). Considering the size, morphology, and localization, we assumed that these spherical structures were bulbs, which have been reported as a differentiated membrane structure in the subregion of the tonoplast from studies on the GFP-linked tonoplast markers γ-TIP and Vam3 (Saito et al., 2002, 2011a). Bulbs have been considered to be double membrane structures in the central vacuole because of their higher fluorescence intensity. In VHP1-GFP plants, the fluorescence ratio of the spherical structures to the tonoplast was more than 3.0 and reached 5.2 in some cases (Figure 3D). These properties indicate that the observed structures are bulbs.

Formation of the Bulb Depends on the Expression Level of VHP1-GFP

Young growing tissues such as the elongating region (hook) of hypocotyls have more H^+-PPase than mature tissues of mung bean (Nakanishi and Maeshima, 1998). In comparison with vacuolar H^+-ATPase, H^+-PPase is the major vacuolar proton pump in dividing and expanding cells, which have a high PPi content (Maeshima, 1990). As estimated, the hook region of hypocotyls and the root tip region in *Arabidopsis* seedlings showed stronger fluorescence than the corresponding mature

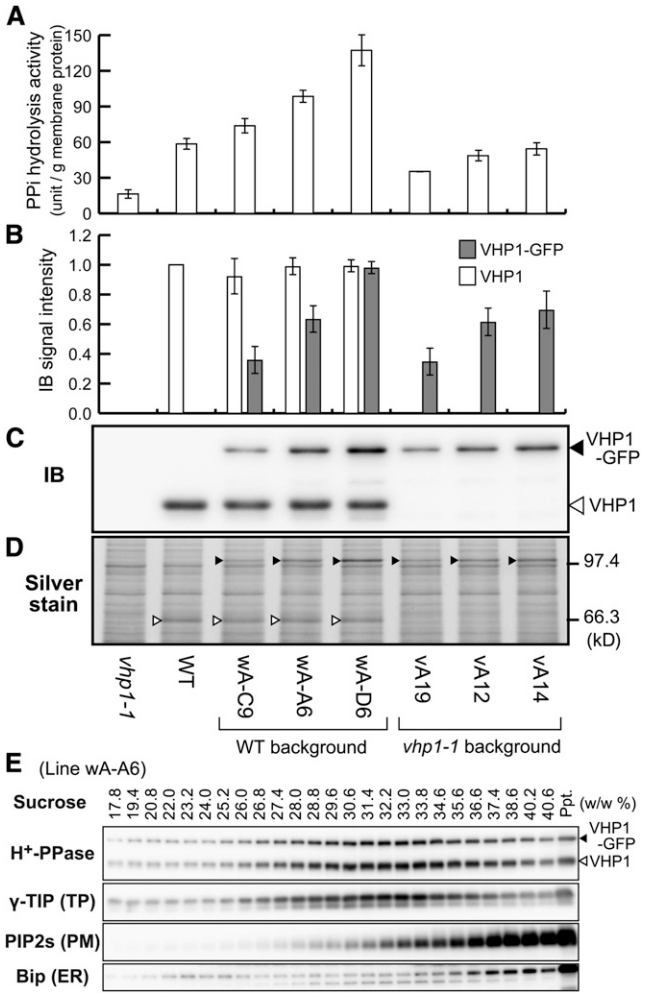

Figure 2. Biochemical Properties of VHP1-GFP-Expressing Lines.

Crude membrane fractions (100,000*g* precipitate) prepared from 9-d-old seedlings of eight lines, *vhp1-1*, wild type (WT), three VHP1-GFP lines inserted into the wild type, and three VHP1-GFP lines inserted into *vhp1-1* were assayed.

(A) PPi hydrolysis activity.

(B) Relative protein content of VHP1 and VHP1-GFP determined by immunoblotting. The amount of VHP1 in the wild type was regarded as 100%. Bars indicate SD from three independent experiments (**[A]** and **[B]**).

(C) An immunoblot with anti-H^+-PPase antibody. Open and closed triangles indicate the position of VHP1 and VHP1-GFP, respectively.

(D) Silver-stained image of the crude membrane fractions (1.0 μg) after SDS-PAGE. VHP1 and VHP1-GFP are marked by open and closed triangles, respectively.

(E) Distribution of VHP1-GFP in sucrose density gradient centrifugation. Crude membrane fractions prepared from intact 3-week-old plants of wA-A6 (VHP1-GFP/wild type) were applied to a sucrose gradient (20 to 40%, w/w). After centrifugation for 18 h, the gradient was fractionated and the concentration of sucrose in each fraction determined. Distribution of H^+-PPase, γ-TIP (tonoplast aquaporin), PIP2s (PM aquaporins), and Bip (ER luminal protein) was determined by immunoblotting with specific antibodies. VHP1-GFP was cofractionated with endogenous H^+-PPase and a tonoplast marker, γ-TIP.

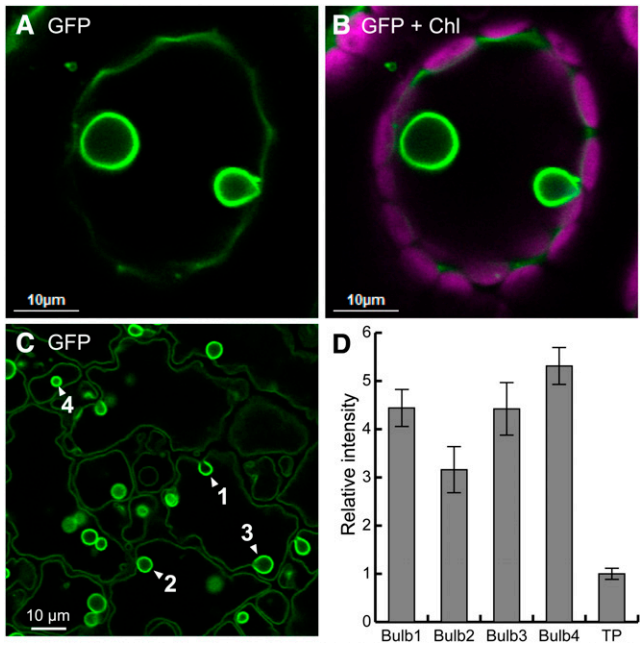

Figure 3. Localization of VHP1-GFP in Membranes of Vacuoles and Bulbs.

(A) A leaf mesophyll cell of the wA-A6 line observed by CLSM. Extracellular air space was filled with water to avoid laser scattering. Two bulbs are shown in a central vacuole.
(B) Merged image of GFP (green) and chloroplast autofluorescence (magenta).
(C) Epidermal cell (abaxial) of a 4-DAG cotyledon of the wA-A6 line.
(D) Fluorescence intensity of bulbs and the tonoplast (TP) from **(C)**. Bars indicate SD calculated from intensities of traced pixels.

regions of hypocotyls and roots (Supplemental Figure 3). These young cells had many bulbs, but no bulbs were observed in tissues with low VHP1-GFP content. Since H+-PPase is the major component of the tonoplast (Maeshima, 2001), the accumulation of excess VHP1-GFP may affect vacuolar morphology.

To investigate the correlation between VHP1-GFP levels and bulb formation, we determined the fluorescence levels in several transgenic lines of both wild-type and *vhp1-1* backgrounds (Figures 2A to 2D) and compared the numbers of bulbs in elongating root cells along a 20- to 40-μm region of the longitudinal axis. In this experiment, we analyzed bulbs that had 3 times greater fluorescence than the normal tonoplast and excluded dividing cells with clustered small vacuoles because of their structural complexity. Bulb formation was positively correlated with the expression of VHP1-GFP (Figures 4A to 4G). Line wA-D6, which showed high expression of VHP1-GFP, had many bulbs compared with wA-A6 and wA-C9, which showed medium and low expression of VHP1-GFP, respectively. Furthermore, it is notable that the endogenous VHP1 level did not affect bulb formation. The vA-12 line expressed VHP1-GFP at a moderate level and formed bulbs even though the line had no endogenous VHP1 (Figures 2B and 4B). Thus, we concluded that bulb formation was due to higher expression of VHP1-GFP.

To confirm our findings, we visualized vacuoles and their related compartments in the wild type by staining with FM4-64 and compared the images with those of transgenic plants expressing VHP1-GFP and *35S^{pro}:GFP-Vam3* (Uemura et al., 2002). Bulbs stained with FM4-64 were detected in the root elongation zone of line wA-A6 expressing VHP1-GFP (Figures 4H to 4J). However, there were no bulbs in the equivalent region of the wild type (Figure 4K). In the *35S^{pro}:GFP-Vam3* lines, there were many bulbs in the lateral root caps (Supplemental Figures 4A to 4G), whereas the wild type had no bulbs.

Moreover, we crossed the wA-A6 line (GFP) with the Vam3^{pro}:mRFP-Vam3 line (Uemura et al., 2010) to generate plants with vacuoles with two-color fluorescence. The transgenic lines showed bulbs both with high green fluorescence of VHP1-GFP and weak purple fluorescence of mRFP-Vam3 (Supplemental Figures 4H to 4J). This result indicates that VHP1-GFP was more highly concentrated in the bulbs than mRFP-Vam3 and suggests that the accumulation of the membrane-anchored GFP in the cells caused bulb formation.

Dimerization of GFP Causes the Formation of Bulbs

At high concentrations, GFP from the jellyfish *Aequorea victoria* tends to form anti-parallel dimers (Yang et al., 1996). Also, pairs of GFP derivatives, such as cyan fluorescent protein (CFP) and YFP, have been reported to cause an artifactual fluorescence resonance energy transfer reaction on membranes (Zacharias et al., 2002). We suspected that one VHP1-GFP interacts via the GFP moiety with a second molecule in a closely apposed tonoplast. Cotyledons of wA-A6 2 d after germination (DAG) had several flat, adhering membranes with high fluorescence (Figure 5D). Flat, adhering double membranes were also observed in lines showing low expression of VHP1-GFP, such as wA-C9 (Figure 5G). In any case, the contact regions showed high fluorescence. In 4-DAG cotyledons of wA-A6 (Figure 5E), spherical bulb structures appeared instead of flat, adhering membranes. Therefore, the flat double-adhered membranes in 2-DAG cotyledons may be precursors of the bulbs found in 4 DAG. Flat, adhering double membranes were also detected in the root tips of wA-A6. Using time-lapse imaging, we observed the fusion of two vacuoles and how the adhering membranes were folded into the vacuolar lumen (Figure 6; Supplemental Movie 1). This may be the initial stage of bulb formation.

To directly test whether bulb formation is caused by GFP dimerization, we used a GFP that does not form a dimer. We exchanged Ala-206 of GFP, which corresponds to Ala-207 of sGFP (Niwa et al. 1999), with a lysine residue (A206K) in the VHP1-GFP construct to prevent dimer formation (Zacharias et al., 2002), and transformed the VHP1-monomeric GFP (mGFP) construct into wild-type plants to obtain wM lines. Although the wM-A9 line expressed VHP1-mGFP at the same level as the wA-A6 line (Figures 5J to 5L), no bulbs were detected in the cotyledon epidermis (Figures 5A to 5C) or in the root elongation zone (Figure 5M). This result demonstrated that bulbs are not formed when GFP is not dimerized.

Conventional CLSM cannot distinguish the two layers of two adhered tonoplasts, which have a thickness of 10 to 20 nm, because the resolution of optical microscopy is ~200 nm (van

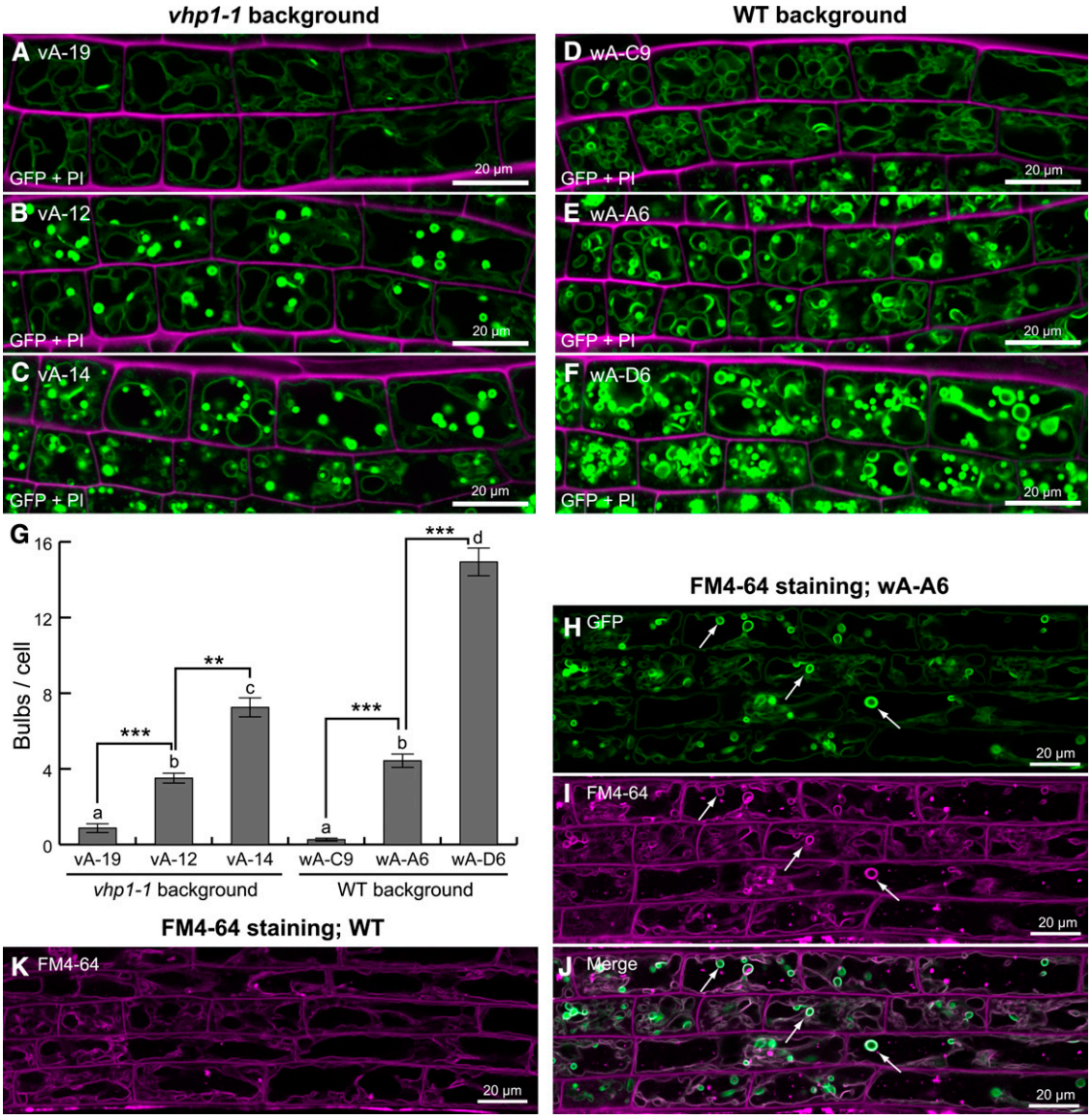

Figure 4. Induction of Bulbs by Accumulation of Membrane-Anchored GFP.

(A) to **(F)** CLSM images of VHP1-GFP (green) and propidium iodide (magenta) of the root elongation zone of 5-DAG seedlings. Plant lines used for each experiment are described by line number. Different lines (vA-19, vA-12, vA-14, wA-C6, wA-A6, and wA-D6) were examined. PI labeled cell wall. vA, *vhp1-1* background; wA, wild-type background.

(G) Number of bulbs in each cell. Spherical structures for which fluorescence was 3 times greater than the tonoplast were counted as bulbs. Root cells with a longitudinal length of 20 to 40 μm were assayed. Bars indicate SE from 69 samples each. The same letter indicates no significant difference at $P > 0.05$. Asterisk indicates significant difference at $^{**}P < 0.001$ or $^{***}P < 0.0001$. Statistical analyses were performed using Steel-Dwass tests.

(H) to **(K)** FM4-64-stained bulbs formed in VHP1-GFP-expressing plants. FM4-64 was used to label plasma membrane and endosomes. Seedlings at 8 DAG were stained with endocytosis tracer FM4-64 for 2 h, washed, and then incubated for 4 h. The elongation zone of the primary root was analyzed by CLSM.

(H) to **(J)** Line wA-A6. In addition to the tonoplast, bulbs (arrows) were also stained with FM4-64 (magenta).

(K) A photograph of a wild-type root stained with FM4-64. There were no bulbs even though the tonoplast was clearly stained. The left side of the photograph corresponds to the root tip.

Putten et al., 2011). Thus, we analyzed the detailed ultrastructure of the bulbs by transmission electron microscopy (TEM). TEM images showed small IVSPs in the wild type, wA-A6, and vA-12. However, the thickness of double membranes observed in wA-A6 and vA-12 was ~70% of those in the wild type (Supplemental Figure 5). The difference was due to the space between the membranes, not to the thickness of the membrane itself. In other words, the membranes adhered more tightly in the bulbs. Therefore, the structures observed in the wild type are different from the bulbs detected in wA-A6 and vA-12 given the thickness of the double membrane.

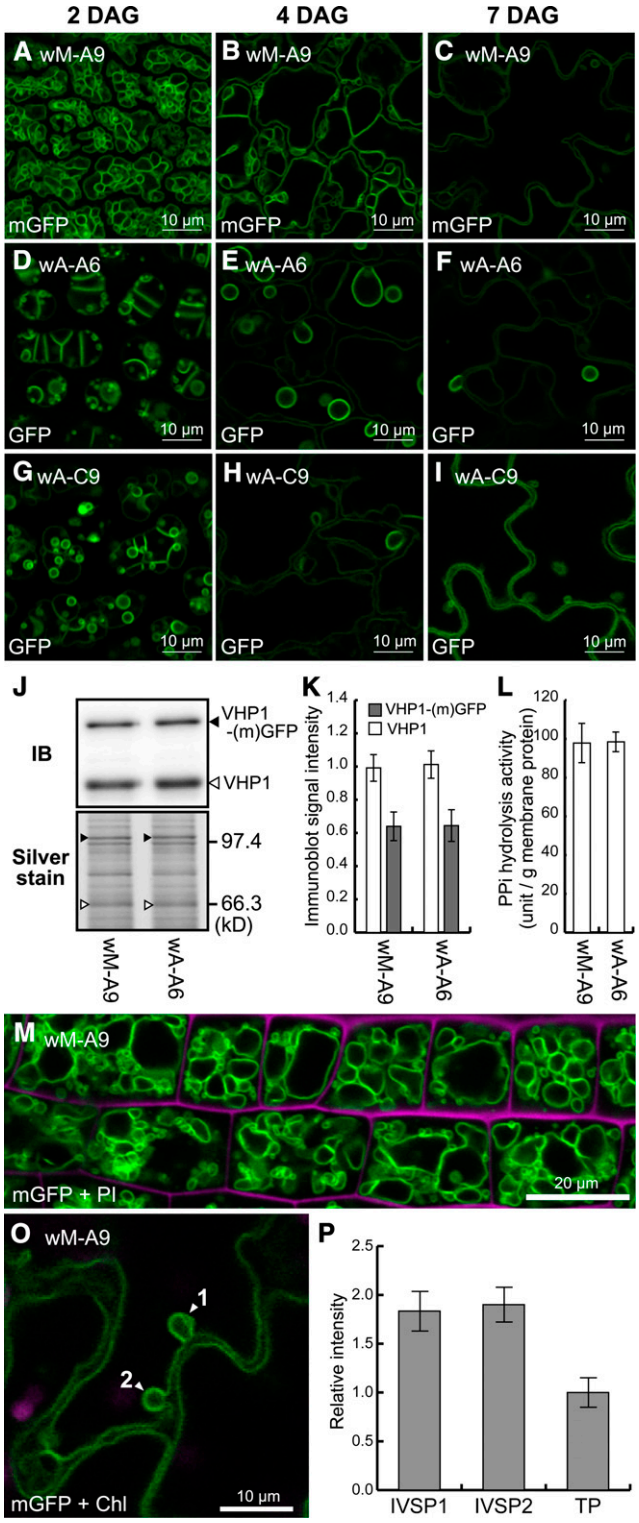

Figure 5. Changes in Bulbs during Maturation of Cells Expressing VHP1 Linked with Dimeric GFP and Disappearance of Bulbs in Cells Expressing VHP1 Linked with Monomeric GFP.

(A) to **(I)** To investigate morphological change in tonoplast, CLSM images of cotyledon epidermal cells (abaxial side) at three growth stages, 2, 4, and 7 DAG, are shown. The appearance of bulbs was compared between transgenic lines expressing monomeric GFP (wM-A9, a middle expression line, **[A]** to **[C]**) and regular dimeric GFP (wA-A6, a middle expression line, **[D]** to **[F]**; wA-C9, a low expression line, **[G]** to **[I]**). Bars = 10 μm.

(J) Immunoblot and silver-stained gel of crude membrane fractions from wM-A9 and wA-A6.

(K) Relative amounts of VHP1 (white boxes) and VHP1-GFP (gray boxes) in wM-A9 and wA-A6 determined by immunoblotting.

(L) PPi hydrolysis activity detected in the crude membranes of wM-A9 and wA-A6. Bars indicate SD from three independent experiments.

(M) CLSM image of mGFP and propidium iodide (magenta, cell wall) of the wM-A9 root elongation zone corresponding to the region shown in Figures 4A to 4F.

(O) IVSPs (arrowheads) found in a wM-A9 cotyledon epidermal cell.

(P) Relative fluorescence intensities of the IVSPs (shown by arrowheads 1 and 2 in **[O]**) and tonoplast (TP). Bars indicate SD calculated from intensities of traced pixels.

In addition to the TEM images of the wild type (Supplemental Figure 5), IVSPs were observed in wM-A9 (VHP1-mGFP) cotyledons by CLSM (Figures 5C and 5O). The fluorescence intensity of the IVSP was just twice that of a single, normal tonoplast (Figures 5O and 5P). On the other hand, bulbs detected in wA-A6 and wA-C9 (VHP1-GFP) showed a fluorescence intensity 3- to 5.4-fold that of a single tonoplast (Figures 3C and 3D). These results suggest that the IVSPs detected in the wild type by TEM and in wM-A9 are different from the bulbs in VHP1-GFP lines such as wA-A6 and vA-12.

Conditions for Tonoplast Adjacency and GFP Dimerization

The results suggest that bulbs are an artifactual structure caused by GFP-GFP antiparallel dimerization as shown in our schematic model (Figure 7). However, it has been speculated that GFP dimerization rarely occurs on the tonoplast because plant vacuoles reportedly are surrounded by actin filaments (Higaki et al., 2006). Therefore, GFP dimerization may not initiate the membrane adjacency but just stabilize membrane adhesion. GFP dimerization might occur under a specific conditions when two membranes are tightly adjacent, e.g., under the conditions of vacuolar fusion. To examine spatiotemporal points of the membrane adjacency and GFP dimerization, we observed the peripheral endosperm cells, which surround the embryo, of water soaked seeds and ovules by CLSM.

During seed germination, small vacuoles are fused and transformed to a giant central vacuole in each cell. In contrast, during seed formation, small vacuoles are kept separate and unfused. We compared both the conditions of maturation and germination of seeds. In peripheral endosperm of seeds of wA-A6, which were imbibed for 4 to 5 h, vacuoles had already bound to each other (Figure 8D) and the most of the cytosolic space was excluded from the membrane-adhered regions. Furthermore, formation of vacuole clusters in the cells also indicated the tight adherence of tonoplasts (Figure 8F; cell space is marked by dotted lines). In contrast, there were many small vacuoles, which were adjacent but not adhering, in cells of wM-A9 (Figure 8A). Furthermore, in ovules of fruits of wA-A6 12 d after flowering (DAF), vacuoles had already bound to neighboring ones (Figure 8H), whereas

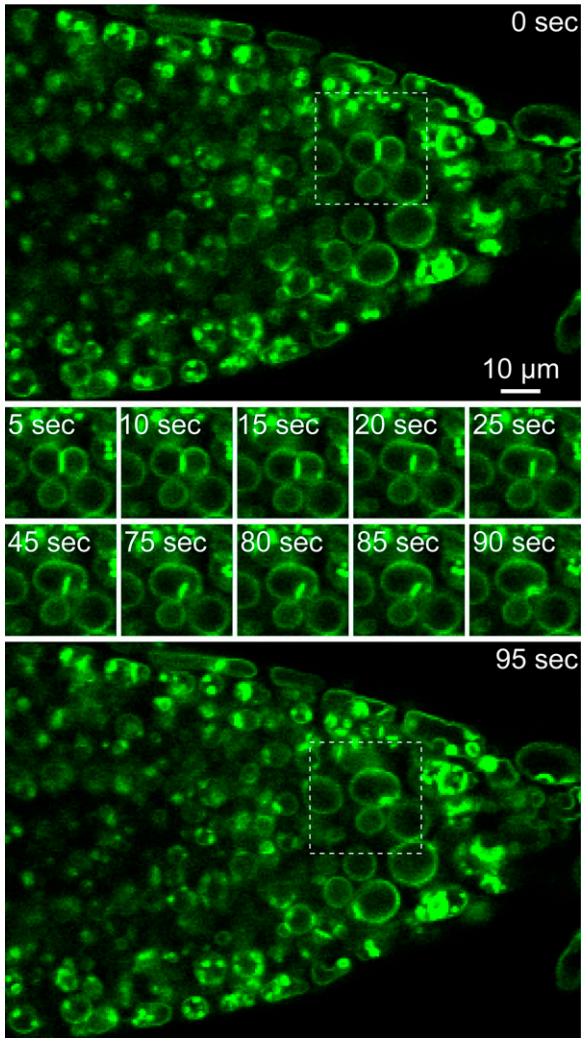

Figure 6. Adhering Membranes Were Folded into the Vacuolar Lumen during Vacuolar Fusion in a wA-A6 Root Tip.

Root tip of VHP1-GFP seedlings (wA-A6) was observed by CLSM. Sheet-like double-membranes (0 s; top panel) were invaginated into the vacuole and then a bulb was observed at 95 s (bottom panel). Pictures in the middle indicate the change of the double membrane to a bulb. For details, see Supplemental Movie 1.

many small vacuoles in wM-A9 kept their spherical shape (Figure 8G). These ovules in maturating seeds were at the stage of predormancy. Therefore, we should note that bulbs could be formed independently of vacuole fusion, as observed in maturing seeds.

Time-Lapse Imaging of Formation and Disappearance of IVSP

As demonstrated above, the IVSPs observed in the wild type (Supplemental Figure 5) and wM-A9 expressing VHP1-mGFP (Figure 5O) have a different structure from bulbs. However, the physiological roles, formation and disappearance of the IVSPs in cells are unclear.

Because of high expression of H^+-PPase, which is a major tonoplast protein that accounts for 10% of the total protein (Maeshima 2001), the fluorescence of VHP-mGFP was notably high compared with other protein components. This property is helpful for advanced microscopy analysis, namely time-lapse 3D imaging. Furthermore, peripheral endosperm cells of seeds highly express VHP1 and maintain their size and positions. These properties of the cells allow time-lapse analysis of their morphology for a relatively long period. To obtain 3D images of vacuoles in peripheral endosperm cells of wM-A9 expressing VHP1-mGFP, we performed four-dimensional analysis, which takes sequential images of Z series, a stack of continuous optical sections through Z axis, by rapid imaging (Figure 9).

Figure 9A (see also Supplemental Movie 2) shows the moment of fusion of two vacuoles. Vacuole a was in contact repeatedly with vacuole b via extension of part of the tonoplast (arrowhead). Then, vacuole a interacted with vacuole c and finally fused with vacuole c within 1 min (arrows). The results indicate the existence of an unknown system by which two vacuoles are pulled and contacted to each other and that the contact is not enough for vacuolar fusion. Thus, tight adhesion of tonoplasts and the vacuolar fusion should be considered separately.

In Figure 9B (see also Supplemental Movie 2), at first, vacuoles d and e were in contact and formed a double membrane with twice the fluorescent intensity of a single tonoplast. Then the two vacuoles fused; however, the double membrane was changed to a tube-like structure (arrows). Finally, the tube-like structure was retransformed to a double membrane (arrowheads) and two vacuoles, d' and e', formed again. A schematic model for this transformation is shown in Figure 9J. This observation suggests a reversible structural change between the tube-like structure and the double-layered membrane.

Figure 9C (see also Supplemental Movie 2) shows the moment of formation of an IVSP in an enfolding vacuole, f, into its neighboring vacuole, g. Before formation of the IVSP, vacuoles f and g were apparently closely attached; then, a part of vacuole f moved to the membrane of vacuole g (arrowhead). Finally, vacuole f was transformed into an IVSP in vacuole g (arrows). During the process, partial membrane fusion might have occurred between vacuoles f and g, based on the observed shrinkage of vacuole f.

Figure 9D (see also Supplemental Movie 3) shows the moment of disappearance of an IVSP. Vacuole h, which included an IVSP, was pulled toward the upper right. Then the IVSP (arrows) was pushed out from vacuole h and transformed into a regular vacuole with a single membrane. Figure 9K shows a schematic model for retransition of an IVSP to a regular vacuole. Reversibility of IVSP formation was not detected in the case of bulbs, which appeared in plants expressing VHP1 linked with regular GFP.

We observed vacuoles in other tissues and found complex, invaginated vacuoles containing many large IVSPs in epidermal cells of pistils taken from open flowers of the wM-A9 line (Figure 9F). For comparison of IVSPs with bulbs, we observed the corresponding cells in wA-A6 (Figure 9G). The bulbs observed in wA-A6 were markedly smaller than the IVSPs in wM-A9, suggesting a difference in their morphology and mechanism of formation. Moreover, wA-A6 had spherical central vacuoles surrounded by a relatively large cytoplasmic space and showed no intravacuolar strands or structure except for small bulbs.

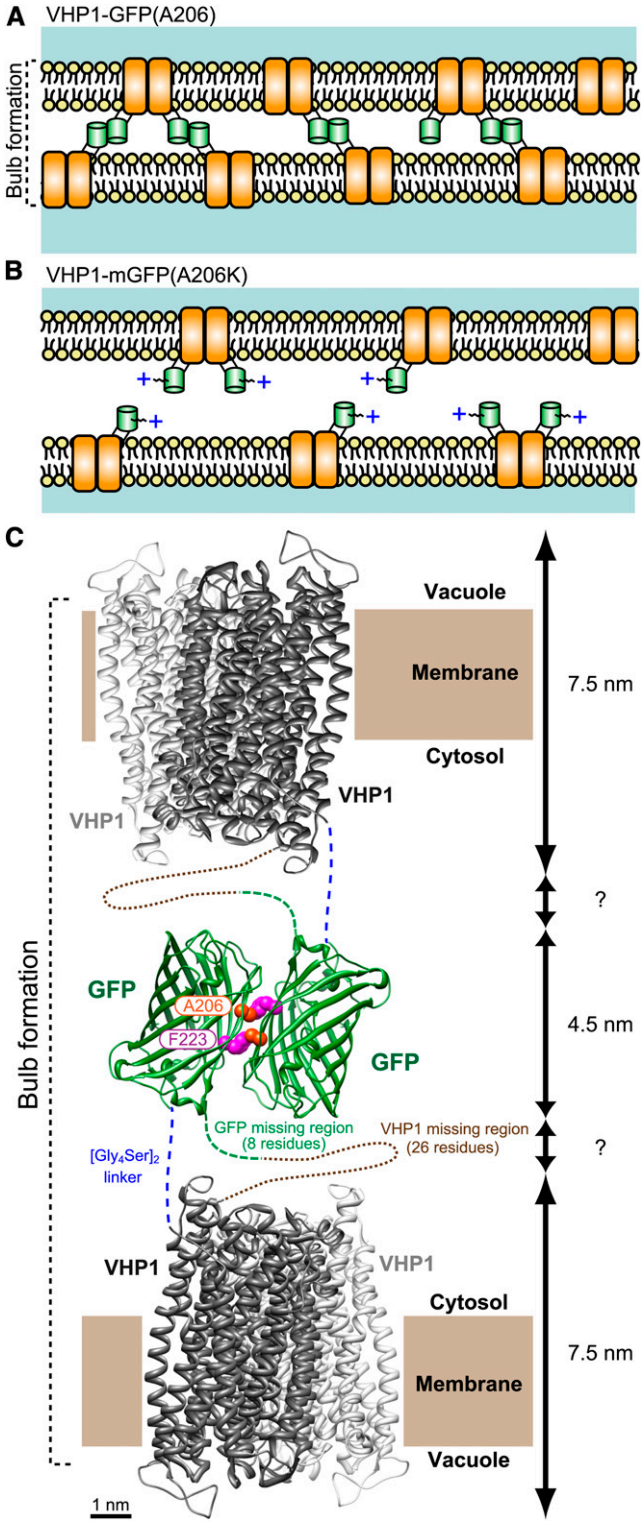

Figure 7. Schematic Model of Tonoplast Adhesion via VHP1-GFP Dimerization.

(A) In VHP1-GFP-expressing cells, VHP1-GFPs form dimers with molecules in the opposite-side membrane and generate bulb structures. In the GFP homodimer, the Ala-206 residue interacts with Phe-223 of its partner GFP by a hydrophobic bond (Yang et al., 1996).

(B) In VHP1-mGFP-expressing cells, the positive charge and steric hindrance of the Lys-206 side chain completely block GFP dimerization. As a result, adjacent tonoplasts are kept at a proper distance from each other.

(C) Schematic model of tonoplast adhesion via VHP1-GFP dimerization. H+-PPase exists as a dimer as shown by Lin et al. (2012) (PDB ID: 4A01; *Vigna radiata* VHP1). The dimeric structure of GFP is taken from PDB ID: 1GFL (Yang et al., 1996). Modeling of the molecular structure of the dimeric form of VHP1-GFP was made with UCSF Chimera software (a visualization system for exploratory research and analysis; www.cgl.ucsf.edu/chimera/download.html). Ala-206 of GFP interacts with Phe-223 in another GFP by a hydrophobic bond, and a homotypic dimer is formed. Total thickness of the double tonoplast is estimated to be around 20 nm when the region of the [Gly_4Ser_2] stacked linker is a few nanometers. This value is comparable to the thickness shown in Supplemental Figure 5J.

These observations suggest that adhesion of tonoplasts through GFP dimerization inhibits the normal dynamic morphological changes of vacuoles.

4D analysis of pistil epidermis of the wM-A9 line showed moments when both an intravacuolar sheet was changed to an IVSP (Figure 9H, arrows; Supplemental Movie 4) and when an IVSP was changed to the sheet-like structure (Figure 9I, arrows; Supplemental Movie 4). The IVSPs detected in pistils may be derived from the intravacuolar sheets. During morphological change of a pistil IVSP (Figure 9I, arrowhead), a pore was generated in the IVSP and then extended in size. As a result, the IVSP changed into a sheet-like structure. Similar pores were observed in intravacuolar sheets, especially in hypocotyl cells, which had complex invaginated vacuoles and IVSPs, as well as pistil epidermis (Supplemental Figure 6 and Supplemental Movie 5). In these cells, the pores were expanded and changed from intravacuolar sheets to transvacuolar strands (Supplemental Figure 6 and Supplemental Movie 5). Therefore, the membrane fusion system may function in the formation of pores and change the dynamics of intravascular sheets.

VHP1 Is Specifically Localized in Tonoplast under Physiological Conditions but Missorted to the PM When Artificially Highly Expressed

H+-PPase has been reported to be localized in the PM in a few, restricted tissues (Robinson et al., 1996; Li et al., 2005). In addition to a strong fluorescent signal in the tonoplast, weak fluorescence was detected in the PM in VHP1-GFP and VHP-mGFP plants when observed by CLSM at high sensitivity. We compared images of the root elongation zones among three VHP1-mGFP lines with different expression levels (Supplemental Figure 7). In wM-B3, which expressed VHP1-mGFP at low levels, fluorescence could not be detected in the PM. On the other hand, clear fluorescence was detected in the PM in the highest expression line wM-A1. These results indicate that H+-PPase is localized only to the tonoplast and that excessive expression of VHP1-mGFP causes mislocalization of part of the protein to the PM.

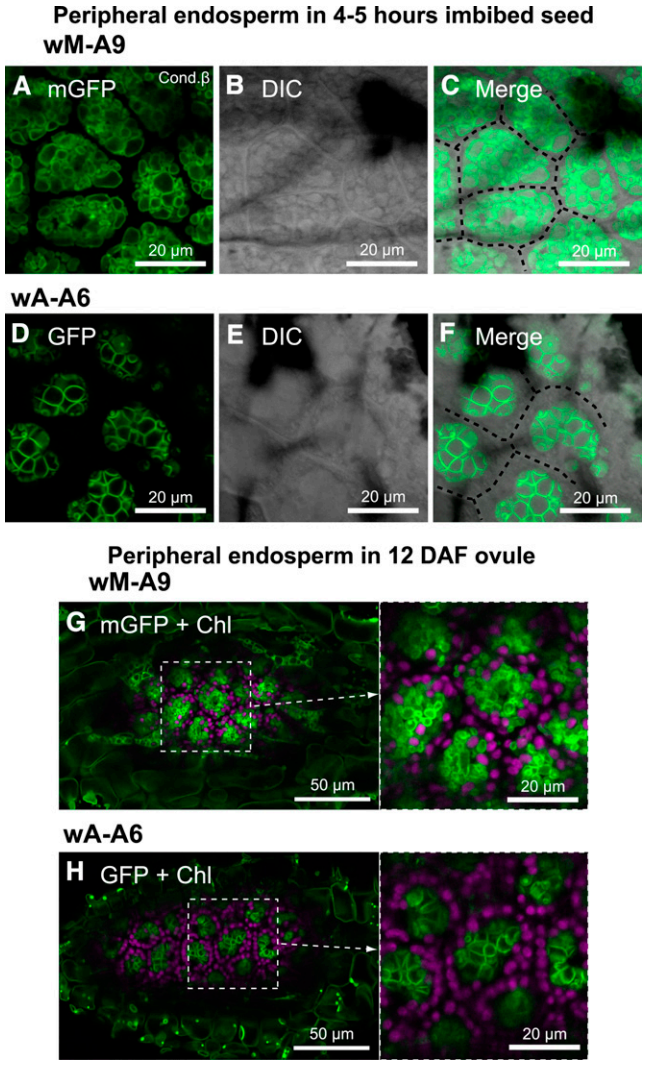

Figure 8. GFP Dimerization Occurring before Seed Maturation in Peripheral Endosperm.

CLSM images of peripheral endosperm were observed in seeds imbibed with water for 4 to 5 h for wM-A9 (**[A]** to **[C]**) or wA-A6 (**[D]** to **[F]**) and immature seed in 12-DAF fruit of wM-A9 **(G)** and wA-A6 **(H)**.

Analysis of Vacuolar Morphology and Accumulation of H^+-PPase Using VHP1-mGFP

In this study, the expression of VHP1-mGFP was controlled under the VHP1's own promoter (Figure 1B), which reflects the normal tissue specificity and expression of VHP1. To identify the morphology of native vacuoles and the accumulation of VHP1 under physiological conditions, we observed various tissues of the VHP1-mGFP expressing lines by CLSM. CLSM has advantages over other analytical methods because it allows temporal and spatial information on the intracellular localization and the accumulation pattern of target proteins in living cells to be obtained.

To quantitatively compare the fluorescence intensity among various organs, images obtained by CLSM were acquired under two conditions: condition α for tissues with weak fluorescence and condition β for that with strong fluorescence. The difference between these conditions was only in the voltage of the photomultiplier tubes, which affected efficiency of photon sensing (condition α, 546 V; condition β, 441 V).

H^+-PPase has been shown to be a major proton pump in dividing and expanding cells because of the high content of PPi in these cells derived from active synthesis of nucleic acids, proteins, and cell wall components based on observation of etiolated hypocotyls (Supplemental Figure 3; Nakanishi and Maeshima 1998). Similarly, high expression of VHP1 was observed in the root tip and root elongation zone (Figures 10A and 10B). Interestingly, stem cells, including the quiescent center, and the first and second cell layers of the columella, which exists in the deep portion of the root tip and has low dividing activity compared with surrounding cells (Dolan et al., 1993), had significantly low fluorescence despite using thin 3-DAG roots (Figure 10F). Similar results were obtained using two-photon excitation microscopy, which is excellent for analysis of deep cells, except for obtaining weak but reliable signals of vacuoles in stem cells (Figure 10E). Furthermore, the fluorescence intensity in the vascular bundle increased after secondary growth (Figures 10G to 10I). We found several IVSPs in TEM images of wild-type root tips (Supplemental Figures 5A to 5C). However, it was difficult to distinguish IVSPs from small vacuoles in root tips and the root elongation zone by CLSM because of the complexity of vacuolar shape in these cells (Figures 10D to 10F).

In petals just after flowering, elongating cells positioned in the middle part of the petal showed strong fluorescence that was twice that in cells of the upper part (Figures 10J to 10L). These observations support the hypothesis that VHP1 expression is correlated with PPi production in plants.

Furthermore, we found a different pattern of VHP1-mGFP accumulation, which may be independent of cell growth. In root vascular bundles before secondary growth, only the phloem companion cells had strong fluorescence (Figures 10H and 10I). Vacuoles in the companion cells showed a relatively complex shape and several bright points, which might be IVSPs. Similarly, petal and leaf veins showed notably high fluorescence of VHP1-mGFP (Figures 10N and 10O), suggesting that H^+-PPase activity is involved in the function of phloem.

Leaf mesophyll cells are covered by nonphotosynthetic epidermal cells. The tonoplast of mesophyll cells showed more than twice the fluorescence of epidermal cells on both the adaxial side (Figure 10M) and abaxial side (Figure 11).

One of the brightest tissues examined was the nectary, which secretes nectar for attraction of pollinators. *Arabidopsis* has lateral and median nectaries (Figures 10R and 10S). Both nectaries gave significantly strong fluorescence. Another tissue, which had a funicle, a bridge between the growing ovule and mother body, also had extremely high fluorescence (Figures 10P and 10Q).

When relative intensity of fluorescence in the tonoplast was compared among various tissues (Figure 11), the values in mesophyll, phloem, nectary and funicle cells as well as growing cells, such as elongating root cells, were higher. These tissues, such as phloem and nectaries, have the common property of providing sugars.

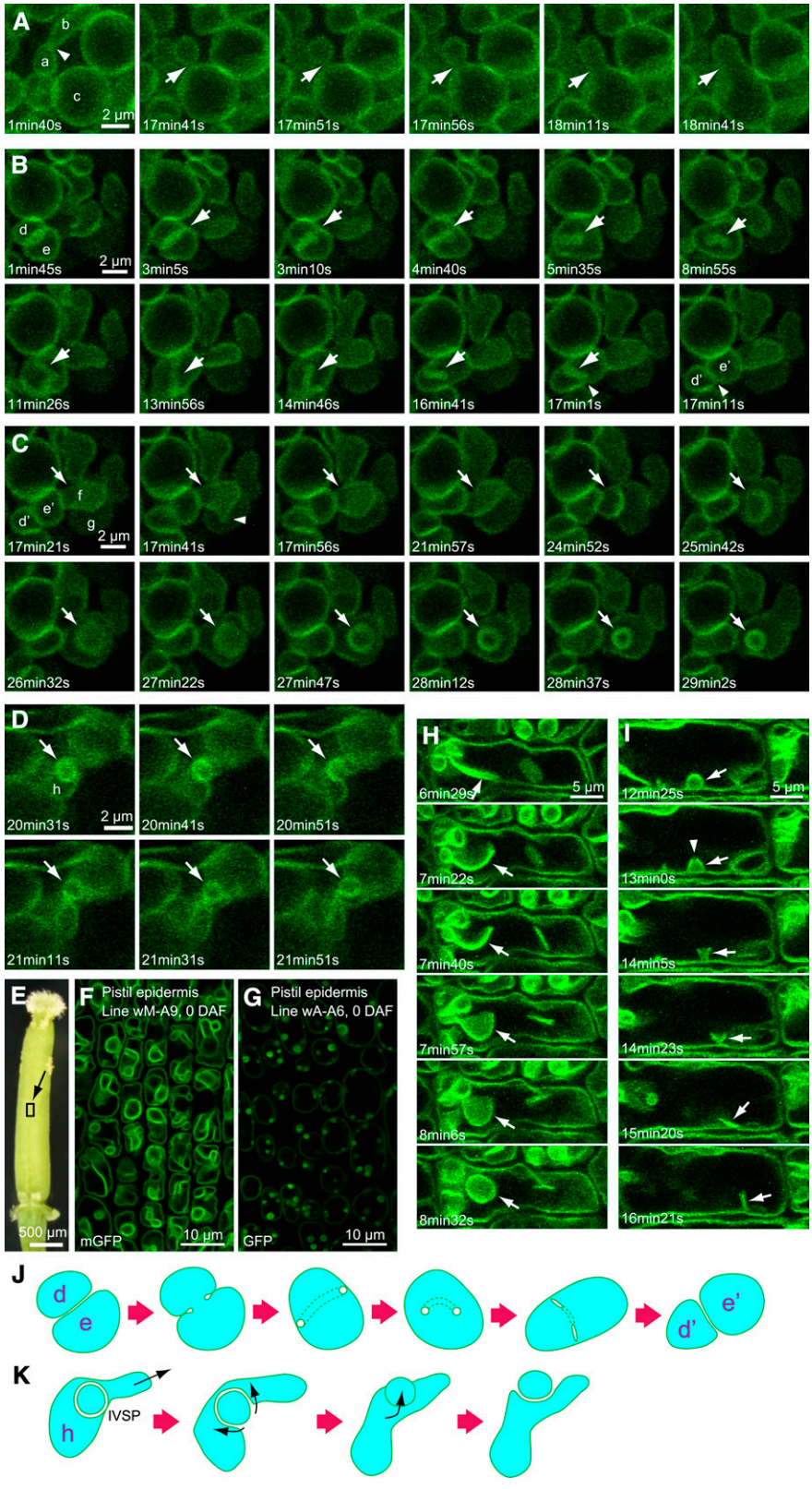

Figure 9. Vacuolar Dynamics Visualized by VHP1-mGFP.

DISCUSSION

Construction of Functional VHP1-GFP

Visualization of proteins has enabled detailed studies in cell biology. In particular, expression of GFP-linked proteins allows their real-time monitoring in living cells and tissues. However, artifactual effects of GFP may be seen in cells. For example, linkage of a large molecule such as GFP may cause dysfunction of enzymes and mislocalization of proteins.

In this study, we prepared a functional H^+-PPase linked with GFP and expressed it under the control of the *VHP1* promoter. VHP1-GFP displayed normal PPi-hydrolysis and proton pump Supplemental Figure 1). By the introduction of H^+-PPase-GFP, the phenotypic properties of *vhp1* or *fugu5*, which has cotyledons more rectangular than the wild type (Ferjani et al., 2011), were recovered (Supplemental Figure 2). Cytoplasmic loop *A*, which was the site of GFP insertion, is the most heterogeneous region of the eight cytoplasmic loops, and its 3D structure has not been determined, indicating that loop *A* does not have a fixed structure. Loop *A* has four characteristic residues, serine, glutamic acid, glutamine, and glycine, which are abundant in intrinsically disordered proteins (Uversky and Dunker, 2010). The structural flexibility of loop *A* probably permits the insertion of GFP without causing dysfunction of H^+-PPase, although the biochemical function of loop *A* is unknown.

GFP Dimerization Triggers Artifactual Adhesion of Tonoplasts and Formation of Bulbs

Bulbs were found in VHP1-GFP-expressing plants. This study revealed that the bulb is an artifactual structure caused by dimerization of GFP. First, the formation of bulbs positively correlated with the amount of VHP1-GFP protein, but not that of endogenous H^+-PPase (Figure 4). Second, the number of bulbs also increased in plants expressing another tonoplast marker linked with GFP (GFP-Vam3; Uemura et al., 2002; Saito et al., 2011a) compared with the wild type (Supplemental Figure 4). Third, no bulbs formed in plants expressing H^+-PPase tagged with the monomeric GFP (VHP1-mGFP) (Figure 5). It is known that GFP has the capacity to form a homodimer by intermolecular hydrophobic and hydrophilic bonds, e.g., between Ala-206 and Phe-223 (Yang et al., 1996). A homotypic interaction of GFPs tagged to H^+-PPase is shown in Figure 7C. Considering their 3D structure, two GFPs on the same membrane cannot interact with each other. However, two GFPs immobilized on tonoplast surfaces that face each other can form a dimer (Figure 7). This may trigger the adherence of the two membranes. In other words, GFP can link to the membrane protein like a hook-and-loop fastener to connect the membranes.

As for the tissue specificity of the bulbs, numerous bulbs were detected in the root elongation zone, cotyledons, and hook of etiolated hypocotyls of VHP1-GFP seedlings (Figures 4 and 5; Supplemental Figure 3B). In epidermal cells of 2-DAG cotyledons (Figure 5D) and peripheral endosperm cells of immature and water imbibed seeds (Figures 8D and 8H), there were sheet-like structures with high fluorescence at the regions of contact of two vacuoles. In root tips, flat, adhering double-membranes were invaginated into the vacuole and became a bulb (Figure 6). These findings suggest that the primary structure of the bulb is generated by artifactual adhesion of tonoplasts.

Dimerization of GFP is considered to be negligible in protein visualization experiments because of its relatively large dissociation constant (K_d = 0.1 mM) (Zacharias et al., 2002). Nevertheless, negative effects of dimerization have been reported. In a fluorescence resonance energy transfer assay for membrane proteins, the heterotypic dimerization of CFP and YFP gives a false positive signal even though there is no interaction with the protein of interest (Zacharias et al., 2002). Overexpression of membrane proteins linked with GFP causes adhesion of peroxisomes, mitochondria, plastids, or ER membranes individually via a weak homotypic interaction of GFP (Lisenbee et al., 2003; Snapp et al., 2003). Based on our findings, we recommend changing GFP and its derivatives to the monomer type by a single amino acid substitution for more accurate analyses of membrane proteins.

Like GFP, other fluorescent proteins may cause artifacts in higher-order membrane structures such as formation of bulbs. A bulb structure with high fluorescence was observed in cells expressing TagRFP-Vam3 (Saito et al., 2011b). TagRFP is a modified red fluorescent protein derived from the sea anemone *Entacmaea quadricolor* (Merzlyak et al., 2007). TagRFP has been reported to exist in monomer form based on gel filtration and seminative gel electrophoresis at protein concentrations up to 10 mg/mL (Merzlyak et al., 2007; Subach et al., 2010). In

Figure 9. (continued).

Peripheral endosperm in a water imbibed seed for 30 h (**[A]** to **[D]**) and epidermal cell of the pistil at 0 DAF (**[E]** and **[F]**) were observed by XYZT analysis. Figures were constructed by projection of Z-stack images with a 0.47-μm interval. Thickness of observed area: 1.41 μm (four stacks) in **(A)** to **(C)**, 1.88 μm (five stacks) in **(D)**. All photographs were taken from the wM-A9 line except for **(G)** (wA-A6).

(A) Vacuolar fusion. Arrows indicate points of vacuole fusion.

(B) Tubular structure (arrows) derived from boundary face between two vacuoles.

(C) IVSP formation by invagination (arrows).

(D) IVSP disappearance. Arrows indicate IVSPs.

(E) 0-DAF pistil.

(F) and **(G)** Observed area is indicated by square located on the style. Pistil epidermal cell of wM-A9 **(F)**. Pistil epidermal cell of wA-A6 **(G)**.

(H) IVSP formation by sheet folding.

(I) IVSP disappearance. Arrows indicate IVSPs.

(J) Schematic model of dynamic transformation of vacuoles shown in **(B)**.

(K) Schematic model of transformation of an IVSP to a regular small vacuole, as shown in **(D)**.

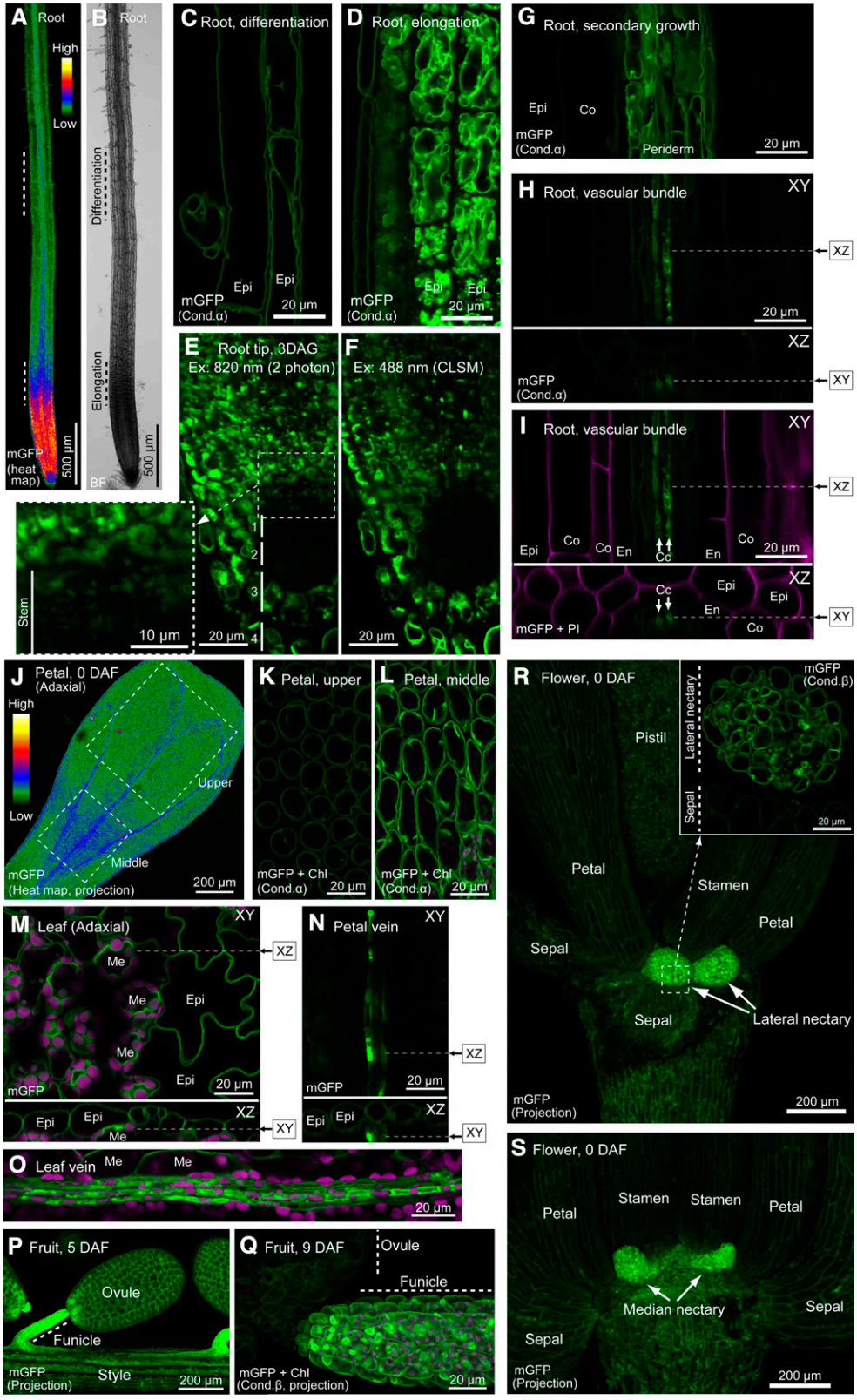

Figure 10. Imaging of VHP1-mGFP in Various Tissues.

contrast, the crystal structure of TagRFP is tetrameric (Subach et al., 2010). Thus, we should consider that bulbs formed in cells expressing TagRFP-tagged membrane proteins are artifacts formed by oligomerization of TagRFP, similarly to proteins tagged with GFP.

GFP Dimerization Is Necessary but Not Sufficient for Bulb Formation

We should note that GFP dimerization is one of the triggers but is not sufficient for bulb formation. These results reveal that formation of bulbs requires three conditions: (1) accumulation of a sufficient amount of a tonoplast protein linked with GFP, (2) surface contact between tonoplasts, and (3) conformational flexibility of GFP linked to the membrane protein for dimerization. H^+-PPase is the major protein component of the tonoplast (Maeshima 2001) and satisfies the requirement (1). Also, this study shows that VHP1-GFP, which has a short flexible linker with 10 amino acid residues, has dimerization capability.

Here, we consider requirement (2). Saito et al. (2011a) showed that cells expressing *Vam3^{pro}:GFP-Vam3* or γ-TIP-GFP have many bulbs and that the number of bulbs was significantly decreased in a *sgr2-1* or *zig-1* background. Mutants *sgr2-1* and *zig-1* lack stem gravitropism due to abnormal vacuolar dynamics that inhibit amyloplast movement in endodermal cells (Morita et al., 2002; Yano et al., 2003). The responsible gene of *zig-1* is Q_b-SNARE VTI11, which encodes a subunit of a connecting complex for membrane fusion. Furthermore, the phospholipase lacking mutant *sgr2* has the defects in physical properties of tonoplasts. Therefore, activity of the SNARE complex and normal properties of tonoplasts might be necessary to form bulbs in GFP-Vam3 plants. These reports and our observations suggest that normal membrane-membrane interaction between two facing tonoplasts under physiological conditions is essential for bulb formation. In other words, the *sgr2-1* and *zig-1* mutants might not satisfy requirement (2).

In a previous report, bulbs were not detected in embryos of early water-imbibed seeds expressing GFP-Vam3 but appeared during germination, when central vacuoles were developed (Saito et al., 2011a). However, we detected primary structures of bulbs even in seeds at the maturation stage, when protein bodies are formed and vacuolar fusion does not occur (Figure 8H). Nevertheless, close contact of tonoplasts was observed in the maturing seeds. Therefore, bulbs tend to be formed during vacuolar fusion and at the moment of relatively stable contact of tonoplast surfaces when GFP-tagged tonoplast proteins are highly expressed.

Properties and Morphological Dynamics of IVSPs

IVSP were found by TEM in wild-type root tips (Supplemental Figure 5) and in cotyledons (Saito et al., 2002). IVSPs were also observed by CLSM in cotyledons (Figure 5C and 5O), petal veins (Figure 10N), funicles (Figure 10Q), peripheral endosperm (Figures 9C and 9D; Supplemental Movies 2 and 3), hypocotyls (Supplemental Figure 7 and Supplemental Movie 5), and epidermis of pistils (Figure 9F). The IVSPs detected by TEM and CLSM were different from bulbs in terms of the thickness of the double membrane (Supplemental Figure 5) and the intensity of fluorescence (Figures 3D and 5P). The thickness of the double membrane of IVSPs was thicker than that of bulbs and the fluorescence intensity of the IVSP membrane was clearly weaker than that of bulbs. The IVSPs and bulbs were found in the same cells of the transgenic plants expressing VHP1-GFP and *Vam3*^{pro}:mRFP-Vam3 (Supplemental Figures 4H to 4J). The observation also strongly suggests that the IVSPs and bulbs were independent structures.

Furthermore, this study clearly showed dynamic morphological changes including transition of small vacuoles to IVSP, exclusion of IVSPs from the host vacuole, and formation of IVSPs from sheet-like structures (Figure 9). Furthermore, our CLSM observations together with previous TEM observations (Saito et al., 2002) revealed the existence of pores in the IVSPs, which

Figure 10. (continued).

(A) Heat map of a root.
(B) Bright field image of **(A)**.
(C) Epidermal cells in root differentiation region.
(D) Epidermal cells in root elongation region.
(E) and **(F)** Root tip of 3-DAG seedling analyzed by two-photon microscopy **(E)** and CLSM **(F)**.
(G) Root vascular bundle during secondary growth.
(H) and **(I)** Vascular bundle of young root. Arrows indicate phloem companion cells.
(J) Heat map of adaxial side of petal at 0 DAF.
(K) Epidermal cells of petal upper region.
(L) Epidermal cells of petal middle region.
(M) Adaxial side of rosette leaf.
(N) Abaxial side of petal, focused on vein.
(O) Abaxial side of rosette leaf. To obtain the vein image, the epidermal layer was peeled off.
(P) Ovule and funicle in 5-DAF fruit.
(Q) Ovule and funicle in 9-DAF fruit.
(R) Bottom of 0-DAF flower. Magnified figure of dashed square is shown at upper right.
(S) Basal region of a flower at 0 DAF.
All mGFP images were obtained by CLSM, except **(E)**, which was obtained by two-photon microscopy. XZ image in **(H)**, **(I)**, **(M)**, and **(N)** was constructed by Z stacking along the dashed line. **(J)**, **(P)**, and **(R)** are projection images of Z-stacks. Epi, epidermis; Me, mesophyll; Co, cortex; En, endodermis; Cc, phloem companion cell.

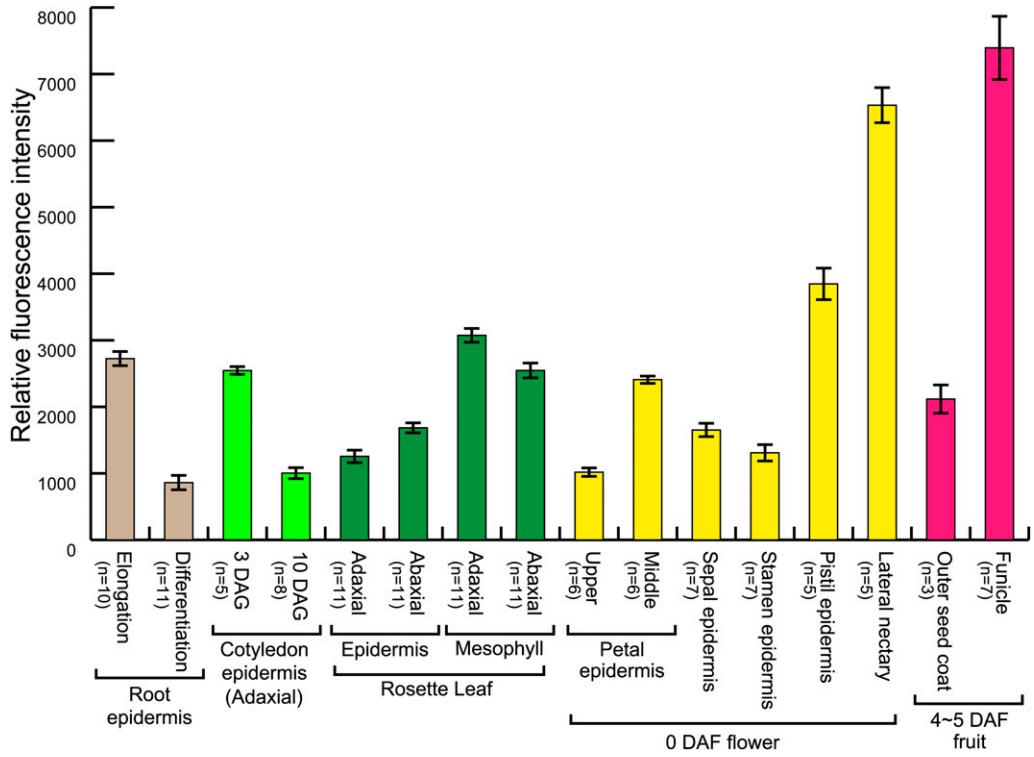

Figure 11. Relative Intensity per Tonoplast of VHP1-mGFP in wM-A9.

The intensities were extracted from CLSM images obtained under two conditions for observation (condition α or condition β; see Methods). Tissues with weak and medium fluorescence were analyzed under the condition α, and the score readout from Fluoview software (Olympus) was defined as the intensity of fluorescence (0 to 4095). Tissues with strong fluorescence were observed under the condition β. Intensity of fluorescence determined under the both conditions was calculated using the same scale. Bars indicate SE. Replication number of each experiment is shown at the left of organs' name.

connect the lumen of IVSPs and their host vacuole. Appearance of pores triggered the change of an IVSP to a sheet-like structure (Figure 9). Although the physiological relevance of the IVSPs remains to be resolved, these observations suggest that they are a transient structure of the vacuole and temporarily store membrane components in elongating cells.

Internalization of boundary membrane was observed at the late stage of vacuole fusion was observed in yeast cells (Wang et al., 2002), in which subunit a of vacuolar H^+-ATPase (Vph1p) and other vacuolar membrane proteins were tagged with a regular GFP. The internalized boundary membranes were estimated to be digested in the vacuole after completion of vacuole fusion. It is unclear whether these intravacuolar structures were spherical structures. This study suggests that these intralumenal membranes found in yeast cells are different from IVSPs because IVSPs are transformed into transvacuolar strands and intravacuolar sheet-like structures.

Dynamics of Vacuoles under Normal Conditions Revealed by VHP1-mGFP

This study on plants expressing VHP1-mGFP revealed the multifaceted morphological dynamics of vacuoles in the peripheral endosperm and pistil epidermis (Figure 9; Supplemental Movies 2 and 3), such as fusion of small vacuoles and subsequent transformation of a single vacuole within 1 min (Figure 9A), reversible changes between vacuoles and tube-like structures within 20 min (Figure 9B), IVSP formation (Figure 9C), reformation of an IVSP to a vacuole within 2 min (Figure 9D), transformation of intravacuolar sheet to IVSP (Figure 9H), and transformation of an IVSP to an intravacuolar sheet (Figure 9I). Considering these results, there might be two mechanisms for formation of IVSPs. IVSPs formed by invagination of neighboring vacuoles in the seed peripheral endosperm and by swelling of intravacuolar sheet-like structures in pistil epidermis. In root tip cells, the 35- to 43-nm double membrane in the wild type was thicker than that of bulbs (Supplemental Figure 5), with just twice the fluorescence intensity of a single tonoplast.

There must be an unknown biochemical mechanism to maintain the membrane thickness without GFP dimerization in IVSPs, intravacuolar sheets, and intravacuolar tube-like structure. The intravacuolar tube-like structures (Figure 9B) might be the transvacuolar strands observed even in the central vacuoles. Transvacuolar strands are lined with actin filaments (Higaki et al., 2006; Oda et al., 2009). Each strand is thought to be created by invagination of a tonoplast groove (Higaki et al., 2006) or by fission of an intravacuolar large membrane sheet (Ruthardt et al., 2005) in tobacco (*Nicotiana tabacum*) BY-2 suspension cells. In *Arabidopsis* hypocotyls, we also observed that several pores in the transvacuolar sheet were expanded and then the sheet was transformed to a transvacuolar strand (Supplemental Figure 6 and Supplemental Movie 5).

In addition to the above morphological changes, this study strongly suggests that the tube-like structures in vacuoles are formed by a mechanism similar to that of the formation of transvacuolar strands from intravacuolar sheets. Tube-like structures developed and eventually separated a single vacuole into two smaller ones, much like a cell plate (Figure 9B). This study revealed that IVSP is another temporal intravacuolar structure in addition to intravacuolar sheets and transvacuolar strands, in the peripheral endosperm, pistil epidermis, and hypocotyl. These dynamic morphological changes of vacuoles cannot be performed only by the tonoplast. Involvement of the cytoskeleton is strongly speculated as reported previously (Higaki et al., 2006; Oda et al., 2009). Further studies using markers for both the tonoplast and actin should provide further insight into the detailed mechanism behind these dynamics.

Marked Accumulation of H^+-PPase in Specific Tissues

H^+-PPase is the main proton pump of the tonoplast in growing tissues, such as growing hypocotyls, which provide a large quantity of PPi through macromolecule biosynthesis (Nakanishi and Maeshima, 1998; Maeshima, 2000). This function was clearly supported by observations that VHP1 was markedly accumulated in root tips, root vascular bundles during secondary growth, growing hypocotyls, young cotyledons, and young petals (Figure 10). In addition to these tissues, marked accumulation of H^+-PPase in funicles, nectaries, leaf mesophyll, and phloem companion cells was clearly demonstrated. The loss-of-function mutant of H^+-PPase and its overexpressing plants should be investigated to shed light on the physiological significance of the enzyme in these cells.

These tissues are rich in sucrose. The tissues with brightest observed fluorescence were the funicle and nectary (Figures 10P to 10S). The main component of nectar in *Arabidopsis* is hexose, which is derived from hydrolysis of sucrose by cell wall invertase and degradation of temporarily stored starch in amyloplasts (Kram and Carter, 2009). Leaf mesophyll cells are the major source of sucrose, which is produced by photosynthesis or degradation of transiently stored starch. Phloem companion cells are a key transport pathway of sucrose from the mesophyll to sieve tubes. High expression of H^+-PPase in the phloem supports previous observations (Mitsuda et al., 2001; Yang et al., 2007; Gaxiola et al., 2012). However, some groups reported that H^+-PPase is localized in the PM of the phloem companion cells and either causes efflux of H^+ to the apoplast to energize a sucrose/H^+ symporter or synthesizes PPi for glycolysis using a proton gradient generated by the P-type H^+-ATPase (Langhans et al., 2001; Paez-Valencia et al., 2011; Gaxiola et al., 2012). This was not confirmed in our observations, since most VHP1-mGFP signals were detected in the tonoplast but not in the PM (Figures 10H, 10I, 10N, and 10O). Thus, the physiological role of H^+-PPase in the PM should be considered.

The common role among the above tissues in which H^+-PPase markedly accumulated is to provide sugars, especially sucrose, to neighboring cells. In metabolic pathways concerned with sucrose or monosaccharide 1-phosphate, PPi is produced or hydrolyzed by reversible reactions catalyzed by UDP-glucose pyrophosphorylase (Park et al., 2010), UDP-sugar pyrophosphatase (Kotake et al., 2007), and PPi-dependent phosphofructokinase (Mustroph et al., 2007). Changes in PPi concentration are known to affect these reactions in a specific direction. Indeed, loss of function of VHP1 caused inhibition of sucrose synthesis from storage oil in seedlings (Ferjani et al., 2011), and heterologous expression of an *Escherichia coli* soluble pyrophosphatase (PPase) in plants increased the content of sugars, starch, and UDP-glucose (Sonnewald, 1992; Geigenberger et al., 1998; Lee et al., 2005). Therefore, a higher level of H^+-PPase might be favorable for synthesis and/or storage of sugars.

Interestingly, Lerchl et al. (1995) revealed that expression of *E. coli* PPase under control of a phloem-specific promoter suppressed transport of sucrose from source leaves to sink tissues and stimulated accumulation of sucrose in the leaves. Moreover, this phenotype was complemented by expression of yeast invertase, which could generate glucose from sucrose for glycolysis. Glycolysis and subsequent oxidative phosphorylation produces ATP for PM H^+-ATPase, which energizes a sucrose/H^+ cotransporter in the PM. Under physiological conditions, sucrose in the companion cells is transported into the sieve elements and also used as a metabolic source for ATP production. This phenomenon seems to be contradictory to high-level expression of H^+-PPase in the companion cells. This difference may be due to the difference in molecular activity between PPase and H^+-PPase because the molecular activity of PPase is 10-fold higher that of the H^+-PPase, although their K_m values for PPi are comparable (Nakanishi et al., 2003; Espiau et al., 2006). High activity of *E. coli* PPase in the transformed companion cells may cause PPi deficiency and suppress hydrolysis of sucrose. As a result, ATP production, which is required for sucrose/H^+ symport, may be strongly reduced. In the case of H^+-PPase, its moderate activity might be efficient for moderate reduction of PPi in companion cells and for a sufficiently high level of sucrose to export to the sieve elements.

In conclusion, the antiparallel dimerization of GFP tagged to H^+-PPase and other membrane intrinsic proteins triggers the generation of artifactual bulbs in young plant cells in which GFP-tagged proteins are highly expressed. This weak homodimerization might have led to misinterpretation of the intracellular morphology of the vacuole and related organelles. Finally, it should be noted that spherical structures are also found in the vacuoles of wild-type tissues, but their structure differed from that of the artifactual bulbs in terms of fluorescence intensity and thickness of the double membrane (Figures 5C and 5O; Supplemental Figure 5). These differences may indicate a difference in the mechanism of membrane adhesion between bulbs and the spherical structures in the wild type. The biological and chemical reasons for the extremely high fluorescence intensity of the adhering membranes remain to be resolved. IVSPs were found in wild-type and VHP1-mGFP-expressing cells such as wM-A9. Although their physiological relevance is unknown, this study strongly suggests reversible transformation between IVSPs, intravacuolar sheet-like structures, and transvacuolar strands. This study also unambiguously shows that H^+-PPase is specifically localized in the tonoplast under physiological conditions but is mistargeted to the PM under conditions of artificially high expression and that H^+-PPase is highly accumulated in sucrose enriched tissues, such as the nectary and funicle, in addition to growing tissues.

METHODS

Plant Materials

Seeds of *Arabidopsis thaliana* (strain, Columbia 0) provided by the RIKEN Bioresource Center were surface sterilized, placed in the dark at 4°C for 2 d, and then sown on half-strength MS-Gellan gum (0.5%; Wako Pure Chemical) plates with 2.5 mM MES-KOH, pH 5.7, and 2% (w/v) sucrose. Plates were incubated for 2 to 3 weeks at 21°C under long-day conditions (16/8 h at 90 μmol m^{-2} s^{-1}). For further analyses, plants were transferred to soil in pots and grown in a greenhouse at 22°C under constant light. The pots were irrigated twice a week with MGRL medium (Naito et al., 1994) containing 1.75 mM sodium phosphate, pH 5.8, 1.5 mM $MgSO_4$, 2.0 mM $Ca(NO_3)_2$, 3.0 mM KNO_3, 12 μM Fe(III)-EDTA, 30 μM H_3BO_3, 10.3 μM $MnSO_4$, 1.0 μM $ZnSO_4$, 1.0 μM $CuSO_4$, 130 nM $CoCl_2$, and 24 nM $(NH_4)_6Mo_7O_{24}$.

Preparation of Constructs of H+-PPase Tagged with GFP

For VHP1-GFP construction, the −1809 to +3071 region of VHP1 was amplified from *Arabidopsis* (ecotype Columbia-0) genomic DNA using KOD FX (Toyobo) with the pair of oligonucleotides, VHP1proFw and VHP1Rv (all primer sequences are listed in Supplemental Table 1). The amplified sequence was cloned into pENTR-D-TOPO (Invitrogen) and its sequence was confirmed. The cloned VHP1 was cut by the inverse PCR method using the following primers: Linker_aLoop1941_Rv and GFP_aLoop1942_Fw. The open reading frame of sGFP was amplified from CaMV35S-sGFP(S65T)-NOS3′ (Niwa et al., 1999) with the pair of oligonucleotides, Linker_GFPM1A_Fw and GFPnonstop_Rv. These DNA fragments were fused using a Clone EZ kit (GenScript). These sequences were confirmed by DNA sequencing. The construct, pENTR-VHP1-GFP, was subcloned into the pGWB401 binary vector (Nakagawa et al., 2007) using Gateway LR Clonase II Enzyme Mix (Invitrogen).

The QuikChange site-directed mutagenesis kit (Stratagene) was used to make VHP1-mGFP as previously described (Mimura et al., 2004). pENTR-VHP1-GFP was mutated using primers sGFP454_A206K_Fw and sGFP618+_A206K_Rv. The pENTR-VHP1-mGFP sequence was confirmed by DNA sequencing and then subcloned into the pGWB501 binary vector (Nakagawa et al., 2007).

Generation of Transgenic Plants

Wild-type and *vhp1-1* plants were transformed by *Agrobacterium tumefaciens* strain C58C1 carrying the VHP1-(m)GFP binary vector by the floral dip method (Clough and Bent, 1998). VHP1-(m)GFP transformants were grown on half-strength MS-Gellan gum plates containing 0.2 mg mL^{-1} Cefotax (Chugai Pharmaceutical). T1 transformants were selected by GFP fluorescence. All transformants used in this study were single T-DNA inserted and homozygous, selected by the segregation ratio of fluorescent pollen and seedlings.

SDS-PAGE and Immunoblotting

Proteins were separated by SDS-PAGE and transferred to an Immobilon-P membrane (Millipore). After treatment with 1% ECL blocking agent (GE Healthcare), the membrane filter was incubated with the primary antibody (1:4000 dilution) and then with horseradish peroxidase-conjugated goat anti-rabbit IgG (1:5000 dilution) (Zymed Laboratories). For H+-PPase detection, we used an antibody to the substrate binding region of H+-PPase that was prepared previously (Segami et al., 2010). The peptide-specific antibodies against *Raphanus sativus* γ-TIP (C+INQNGHEQLPTTDY) and PIP2s (MAKD-VEAVSGEGFQTRDYQDP+C), and *Arabidopsis* Bip (SKDNKALGKLRRE+C) were also prepared previously (Suga et al., 2001; Suga and Maeshima, 2004; Segami et al., 2010). Chemiluminescent reagent ECL (GE Healthcare) was used for detection of antigens. Chemiluminescence was detected with a Light-Capture II imaging device with a cooled CCD camera (Atto).

Protein and Enzyme Assays

The protein content was quantified using a Bio-Rad protein assay kit. PPi hydrolysis was measured at 30°C as described previously (Maeshima and Yoshida, 1989). The assay medium for PPi hydrolysis activity contained 1 mM $MgCl_2$, 1 mM Na_4PPi, 1 mM Na_2MoO_4, 50 mM KCl, 30 mM Tris-MES, pH 7.2, and 0.02% Triton X-100.

Subcellular Fractionation of *Arabidopsis*

A crude membrane fraction was prepared from *Arabidopsis* plants as described previously (Kobae et al., 2004). Three-week-old plants were homogenized at 4°C in a mortar and pestle in a 3× volume of homogenizing medium, which contained 0.25 M sorbitol, 50 mM Tris-acetate, pH 7.5, 1 mM EGTA-Tris, 1% polyvinylpyrrolidone, 2 mM DTT, and protease inhibitor cocktail (1× Complete, EDTA-free; Roche Applied Science). The tissue homogenate was filtered and then centrifuged at 10,000*g* for 10 min at 4°C. The supernatant was centrifuged at 100,000*g* for 30 min at 4°C. The pellet was suspended in 20 mM Tris-acetate, pH 7.5, 0.25 M sorbitol, 1 mM EGTA-Tris, 1 mM $MgCl_2$, 2 mM DTT, and 1× protease inhibitor cocktail and used as the crude membrane fraction.

For sucrose density gradient centrifugation, the crude membrane suspension (2 mg protein, 0.3 mL) was layered on a sucrose density gradient (10 mL of a gradient of 20 to 40% [w/w], 0.7 mL of 50% [w/w] sucrose cushion), centrifuged at 25,000 rpm at 4°C for 18 h in a swinging-bucket rotor (SW41Ti; Beckman Coulter), and collected in 0.42-mL fractions. The sucrose solution consisted of 20 mM Tris-HCl, pH 7.5, 0.5 mM EGTA-Tris, 2 mM $MgCl_2$, and protease inhibitor cocktail.

Microscopy

CLSM observations were conducted with an upright or inverted FV1000-D confocal laser scanning microscope (Olympus). Excitation wavelength and transmission range for emission were 473 nm/485 to 560 nm or 488 nm/500 to 560 nm for GFP and mGFP, 473 nm/617 to 717 nm for propidium iodide, 488 nm/635 to 680 nm for *N*-(3-triethylammoniumpropyl)-4-(6-(4-(diethylamino)phenyl)hexatrienyl)pyridinium dibromide (FM4-64; Invitrogen), 473 nm/660 to 720 nm for chlorophyll, and 559 nm/570 to 670 nm for mRFP. The images were obtained using Olympus Fluoview software and a UPLSAPO60XW water immersion objective or UPLSAPO10X objective lens (Olympus). To quantify the amount of VHP1-mGFP in tissues, CLSM parameters were fixed under two conditions as described below: 3% of 473-nm laser transmissivity, 546 V (condition α) or 441 V (condition β) of photomultiplier voltage, 10.0 μs/pixel of sampling speed, 1024 × 1024 pixel of image size, and UPLSAPO 60XW objective lens. Fluorescent intensity was obtained using Fluoview software by tracing the boundary of membranes in the image.

The intensities were extracted from CLSM images obtained under two conditions for observation (condition α or condition β). Tissues with weak and medium fluorescence were analyzed under the condition α, and the score readout from Fluoview software (Olympus) was defined as the intensity of fluorescence (0 to 4095). Tissues with strong fluorescence were observed under the condition β. Intensity of fluorescence determined under the both conditions was calculated using the same scale. To compare the fluorescent intensity of GFP among several tissues, the fluorescence was normalized with the following equation.

$$F_\beta = (F_\alpha - F_{background})/4.3 + F_{background}$$

where, $F\alpha$ and $F\beta$ are fluorescence detected under the condition α and β, respectively, and $F_{background}$ is the background fluorescence (140 in this experiment) under the condition. The coefficient 4.3 in the equation was calculated from the values taken by comparison of mesophyll tonoplast fluorescence acquired under the condition α and β (n = 30).

Two-photon excitation microscopy observation was conducted with an LSM 780-DUO- NLO instrument (Zeiss). Excitation wavelength for mGFP was 820 nm. Images were obtained by C-Apochromat 40×/1.20 W Korr M27 water immersion objective lens (Zeiss).

Staining of Tonoplast

To visualize the tonoplast in the root elongation zone, seedlings at 8 DAG were suspended in a dye solution containing 20 μM FM4-64, 0.5× Murashige and Skoog salts, 2% sucrose, and 2.5 mM MES-KOH, pH 5.7. The plants were stained for 2 h with gentle agitation in the dark, washed three times, incubated for 4 h with wash solution containing 0.5× Murashige and Skoog salts, 2% sucrose, and 2.5 mM MES-KOH, pH 5.7, and then observed.

See Supplemental Methods for a description of suspension cell culture establishment, tonoplast preparation, H^+ pumping assay, and electron microscopy.

Accession Numbers

Sequence data from this article can be found in the GenBank/EMBL/DDBJ libraries under the following accession numbers: *Arabidopsis* gene of VHP1 (At1g15690.1), VHP2;1 (At1g78920.1), Vam3 (At5g46860), and Bip (At5g42020), and genes for H^+-PPase of *Vigna radiata* (AB009077.1), *Oryza sativa* (Os06g0644200), *Chlamydomonas reinhardtii* (AJ304836.1), *Plasmodium falciparum* (AF115766.1), *Rhodospirillum rubrum* (AF044912.1), and *Streptomyces coelicolor* (AB180905.1).

Supplemental Data

The following materials are available in the online version of this article.

Supplemental Figure 1. H^+-Pump Activity of VHP1-GFP Expressed in Loss-of-Function Mutant *vhp1*.

Supplemental Figure 2. The Heterologous Expression of VHP1-GFP Rescues Rectangular Cotyledon Phenotype of *vhp1*.

Supplemental Figure 3. Numerous Bulbs Were Detected in Dividing and Elongating Cells, Which Expressed VHP1-GFP at High Levels.

Supplemental Figure 4. Bulbs Detected in $35S^{pro}$:GFP-Vam3 Expressing Lines by Staining with FM4-64.

Supplemental Figure 5. Comparison of Bulbs in a VHP1-GFP-Expressing Line and Spherical Structures in the Wild Type by Electron Microscopy.

Supplemental Figure 6. Intravacuolar Structures in Hypocotyls.

Supplemental Figure 7. Mislocalization of VHP1-mGFP to PM Was Observed Only in Lines with High Expression of VHP1-mGFP.

Supplemental Table 1. List of Oligonucleotide Primers.

Supplemental Movie 1. Adhering Membranes Were Folded into the Vacuolar Lumen during Vacuolar Fusion in a wA-A6 Root Tip (Movie Corresponds to Figure 6).

Supplemental Movie 2. Dynamic Changes in Vacuoles Corresponding to Figures 8A to 8C.

Supplemental Movie 3. Dynamic Changes in Vacuoles Corresponding to Figure 8D.

Supplemental Movie 4. Dynamic Changes in Vacuoles Corresponding to Figures 8H and 8I.

Supplemental Movie 5. Dynamic Changes in Vacuoles Corresponding to Supplemental Figures 6C and 6D.

Supplemental Methods.

Supplemental References.

ACKNOWLEDGMENTS

We thank Karin Schumacher (University of Heidelberg) for her critical reading and valuable comments, Yoichi Nakanishi (Nagoya University) for providing *vhp1-1* seeds, Ali Ferjani (Tokyo Gakugei University) for providing *fugu5-1* seeds and critical reading of the article, Tsuyoshi Nakagawa (Shimane University) for providing binary vectors of pGWB401 and pGWB501, Masa H. Sato for providing $35S^{pro}$:GFP-Vam3, Takashi Ueda and Tomohiro Uemura for providing $Vam3^{pro}$:mRFP-Vam3 seeds, and Tetsuro Mimura for critical reading of the article. This work was supported by Grants-in-Aid for Scientific Research from the Ministry of Education, Sports, Culture, Science, and Technology of Japan (23248017, 24114706, and 26252011) and the Steel Foundation for Environmental Protection Technology (2010-29) to M.M. Creation of molecular graphics and analyses were performed with the UCSF Chimera package (www.cgl.ucsf.edu/chimera/download.html). The Chimera was developed by the Resources for Biocomputing, Visualization, and Informatics at the University of California, San Francisco (supported by NIGMS P41-GM103311). Two-photon excitation microscopy observation was supported by the Japan Advanced Plant Science Network (supported by JSPS).

AUTHOR CONTRIBUTIONS

S.S. and M.M. designed the experiments and wrote and finalized the article. S.S. conducted the biochemical and physiological analyses. S.M., A.M., and M.A. performed microscopy observations.

Received May 12, 2014; revised June 30, 2014; accepted July 25, 2014; published August 12, 2014.

REFERENCES

Beebo, A., Thomas, D., Der, C., Sanchez, L., Leborgne-Castel, N., Marty, F., Schoefs, B., and Bouhidel, K. (2009). Life with and without AtTIP1;1, an Arabidopsis aquaporin preferentially localized in the apposing tonoplasts of adjacent vacuoles. Plant Mol. Biol. **70:** 193–209.

Clough, S.J., and Bent, A.F. (1998). Floral dip: a simplified method for *Agrobacterium*-mediated transformation of *Arabidopsis thaliana.* Plant J. **16:** 735–743.

Dolan, L., Janmaat, K., Willemsen, V., Linstead, P., Poethig, S., Roberts, K., and Scheres, B. (1993). Cellular organisation of the *Arabidopsis thaliana* root. Development **119:** 71–84.

Drozdowicz, Y.M., and Rea, P.A. (2001). Vacuolar H^+ pyrophosphatases: from the evolutionary backwaters into the mainstream. Trends Plant Sci. **6:** 206–211.

Escobar, N.M., Haupt, S., Thow, G., Boevink, P., Chapman, S., and Oparka, K. (2003). High-throughput viral expression of cDNA-green fluorescent protein fusions reveals novel subcellular addresses and identifies unique proteins that interact with plasmodesmata. Plant Cell **15:** 1507–1523.

Espiau, B., Lemercier, G., Ambit, A., Bringaud, F., Merlin, G., Baltz, T., and Bakalara, N. (2006). A soluble pyrophosphatase, a key enzyme for polyphosphate metabolism in *Leishmania.* J. Biol. Chem. **281:** 1516–1523.

Ferjani, A., Segami, S., Horiguchi, G., Muto, Y., Maeshima, M., and Tsukaya, H. (2011). Keep an eye on PPi: the vacuolar-type H^+-pyrophosphatase regulates postgerminative development in Arabidopsis. Plant Cell **23:** 2895–2908.

Gattolin, S., Sorieul, M., Hunter, P.R., Khonsari, R.H., and Frigerio, L. (2009). In vivo imaging of the tonoplast intrinsic protein family in Arabidopsis roots. BMC Plant Biol. **9:** 133–141.

Gaxiola, R.A., Palmgren, M.G., and Schumacher, K. (2007). Plant proton pumps. FEBS Lett. **581:** 2204–2214.

Gaxiola, R.A., Sanchez, C.A., Paez-Valencia, J., Ayre, B.G., and Elser, J.J. (2012). Genetic manipulation of a "vacuolar" H+-PPase: from salt tolerance to yield enhancement under phosphorus-deficient soils. Plant Physiol. **159:** 3–11.

Geigenberger, P., Hajirezaei, M., Geiger, M., Deiting, U., Sonnewald, U., and Stitt, M. (1998). Overexpression of pyrophosphatase leads to increased sucrose degradation and starch synthesis, increased activities of enzymes for sucrose-starch interconversions, and increased levels of nucleotides in growing potato tubers. Planta **205:** 428–437.

Hicks, G.R., Rojo, E., Hong, S., Carter, D.G., and Raikhel, N.V. (2004). Geminating pollen has tubular vacuoles, displays highly dynamic vacuole biogenesis, and requires VACUOLESS1 for proper function. Plant Physiol. **134:** 1227–1239.

Higaki, T., Kutsuna, N., Okubo, E., Sano, T., and Hasezawa, S. (2006). Actin microfilaments regulate vacuolar structures and dynamics: dual observation of actin microfilaments and vacuolar membrane in living tobacco BY-2 Cells. Plant Cell Physiol. **47:** 839–852.

Hunter, P.R., Craddock, C.P., Di Benedetto, S., Roberts, L.M., and Frigerio, L. (2007). Fluorescent reporter proteins for the tonoplast and the vacuolar lumen identify a single vacuolar compartment in Arabidopsis cells. Plant Physiol. **145:** 1371–1382.

Katoh, K., Misawa, K., Kuma, K., and Miyata, T. (2002). MAFFT: a novel method for rapid multiple sequence alignment based on fast Fourier transform. Nucleic Acids Res. **30:** 3059–3066.

Kobae, Y., Uemura, T., Sato, M.H., Ohnishi, M., Mimura, T., Nakagawa, T., and Maeshima, M. (2004). Zinc transporter of *Arabidopsis thaliana* AtMTP1 is localized to vacuolar membranes and implicated in zinc homeostasis. Plant Cell Physiol. **45:** 1749–1758.

Kotake, T., Hojo, S., Yamaguchi, D., Aohara, T., Konishi, T., and Tsumuraya, Y. (2007). Properties and physiological functions of UDP-sugar pyrophosphorylase in *Arabidopsis.* Biosci. Biotechnol. Biochem. **71:** 761–771.

Kram, B.W., and Carter, C.J. (2009). *Arabidopsis thaliana* as a model for functional nectary analysis. Sex. Plant Reprod. **22:** 235–246.

Langhans, M., Ratajczak, R., Lützelschwab, M., Michalke, W., Wächter, R., Fischer-Schliebs, E., and Ullrich, C.I. (2001). Immunolocalization of plasma-membrane H+-ATPase and tonoplast-type pyrophosphatase in the plasma membrane of the sieve element-companion cell complex in the stem of *Ricinus communis* L. Planta **213:** 11–19.

Lee, J.W., Lee, D.S., Bhoo, S.H., Jeon, J.S., Lee, Y.H., and Hahn, T.R. (2005). Transgenic *Arabidopsis* plants expressing *Escherichia coli* pyrophosphatase display both altered carbon partitioning in their source leaves and reduced photosynthetic activity. Plant Cell Rep. **24:** 374–382.

Lerchl, J., Geigenberger, P., Stitt, M., and Sonnewald, U. (1995). Impaired photoassimilate partitioning caused by phloem-specific removal of pyrophosphate can be complemented by a phloem-specific cytosolic yeast-derived invertase in transgenic plants. Plant Cell **7:** 259–270.

Lewis, V.A., Basso, L., Blake, N., Salo, J., Lund, T.C., McIvor, R.S., and Orchard, P.J. (2003). Human nerve growth factor receptor and cytosine deaminase fusion genes. Hum. Gene Ther. **14:** 1009–1016.

Li, J., et al. (2005). *Arabidopsis* H+-PPase AVP1 regulates auxin-mediated organ development. Science **310:** 121–125.

Lin, S.M., Tsai, J.Y., Hsiao, C.D., Huang, Y.T., Chiu, C.L., Liu, M.H., Tung, J.Y., Liu, T.H., Pan, R.L., and Sun, Y.J. (2012). Crystal structure of a membrane-embedded H+-translocating pyrophosphatase. Nature **484:** 399–403.

Lisenbee, C.S., Karnik, S.K., and Trelease, R.N. (2003). Overexpression and mislocalization of a tail-anchored GFP redefines the identity of peroxisomal ER. Traffic **4:** 491–501.

Maeshima, M. (1990). Development of vacuolar membranes during elongation of cells in mung bean hypocotyls. Plant Cell Physiol. **31:** 311–317.

Maeshima, M. (2000). Vacuolar H+-pyrophosphatase. Biochim. Biophys. Acta **1465:** 37–51.

Maeshima, M. (2001). TONOPLAST TRANSPORTERS: Organization and function. Annu. Rev. Plant Physiol. Plant Mol. Biol. **52:** 469–497.

Maeshima, M., and Yoshida, S. (1989). Purification and properties of vacuolar membrane proton-translocating inorganic pyrophosphatase from mung bean. J. Biol. Chem. **264:** 20068–20073.

Martinoia, E., Maeshima, M., and Neuhaus, H.E. (2007). Vacuolar transporters and their essential role in plant metabolism. J. Exp. Bot. **58:** 83–102.

Merzlyak, E.M., Goedhart, J., Shcherbo, D., Bulina, M.E., Shcheglov, A.S., Fradkov, A.F., Gaintzeva, A., Lukyanov, K.A., Lukyanov, S., Gadella, T.W., and Chudakov, D.M. (2007). Bright monomeric red fluorescent protein with an extended fluorescence lifetime. Nat. Methods **4:** 555–557.

Mimura, H., Nakanishi, Y., Hirono, M., and Maeshima, M. (2004). Membrane topology of the H+-pyrophosphatase of *Streptomyces coelicolor* determined by cysteine-scanning mutagenesis. J. Biol. Chem. **279:** 35106–35112.

Mitsuda, N., Takeyasu, K., and Sato, M.H. (2001). Pollen-specific regulation of vacuolar H+-PPase expression by multiple *cis*-acting elements. Plant Mol. Biol. **46:** 185–192.

Morita, M.T., Kato, T., Nagafusa, K., Saito, C., Ueda, T., Nakano, A., and Tasaka, M. (2002). Involvement of the vacuoles of the endodermis in the early process of shoot gravitropism in *Arabidopsis*. Plant Cell **14:** 47–56.

Mustroph, A., Sonnewald, U., and Biemelt, S. (2007). Characterisation of the ATP-dependent phosphofructokinase gene family from *Arabidopsis thaliana.* FEBS Lett. **581:** 2401–2410.

Naito, S., Hirai, M.Y., Chino, M., and Komeda, Y. (1994). Expression of a soybean (*Glycine max* L. Merr.) seed storage protein gene in transgenic *Arabidopsis thaliana* and its response to nutritional stress and to abscisic acid mutations. Plant Physiol. **104:** 497–503.

Nakagawa, T., et al. (2007). Improved Gateway binary vectors: high-performance vectors for creation of fusion constructs in transgenic analysis of plants. Biosci. Biotechnol. Biochem. **71:** 2095–2100.

Nakanishi, Y., and Maeshima, M. (1998). Molecular cloning of vacuolar H+-pyrophosphatase and its developmental expression in growing hypocotyl of mung bean. Plant Physiol. **116:** 589–597.

Nakanishi, Y., Yabe, I., and Maeshima, M. (2003). Patch clamp analysis of a H+ pump heterologously expressed in giant yeast vacuoles. J. Biochem. **134:** 615–623.

Niwa, Y., Hirano, T., Yoshimoto, K., Shimizu, M., and Kobayashi, H. (1999). Non-invasive quantitative detection and applications of non-toxic, S65T-type green fluorescent protein in living plants. Plant J. **18:** 455–463.

Oda, Y., Higaki, T., Hasezawa, S., and Kutsuna, N. (2009). New insight into plant vacuolar structure and dynamics. Intl. Rev. Cell Mol. Biol. **277:** 103–135.

Paez-Valencia, J., Patron-Soberano, A., Rodriguez-Leviz, A., Sanchez-Lares, J., Sanchez-Gomez, C., Valencia-Mayoral, P., Diaz-Rosas, G., and Gaxiola, R. (2011). Plasma membrane localization of the type I H+-PPase AVP1 in sieve element-companion cell complexes from *Arabidopsis thaliana.* Plant Sci. **181:** 23–30.

Park, J.I., Ishimizu, T., Suwabe, K., Sudo, K., Masuko, H., Hakozaki, H., Nou, I.S., Suzuki, G., and Watanabe, M. (2010). UDP-glucose pyrophosphorylase is rate limiting in vegetative and reproductive phases in *Arabidopsis thaliana.* Plant Cell Physiol. **51:** 981–996.

Reisen, D., Marty, F., and Leborgne-Castel, N. (2005). New insights into the tonoplast architecture of plant vacuoles and vacuolar dynamics during osmotic stress. BMC Plant Biol. **5:** 13.

Robinson, D.G., Haschke, H.P., Hinz, G., Hoh, B., Maeshima, M., and Marty, F. (1996). Immunological detection of tonoplast polypeptides in the plasma membrane of pea cotyledons. Planta **198:** 95–103.

Ruthardt, N., Gulde, N., Spiegel, H., Fischer, R., and Emans, N. (2005). Four-dimensional imaging of transvacuolar strand dynamics in tobacco BY-2 cells. Protoplasma **225:** 205–215.

Saito, C., Ueda, T., Abe, H., Wada, Y., Kuroiwa, T., Hisada, A., Furuya, M., and Nakano, A. (2002). A complex and mobile structure forms a distinct subregion within the continuous vacuolar membrane in young cotyledons of Arabidopsis. Plant J. **29:** 245–255.

Saito, C., Uemura, T., Awai, C., Tominaga, M., Ebine, K., Ito, J., Ueda, T., Abe, H., Morita, M.T., Tasaka, M., and Nakano, A. (2011a). The occurrence of 'bulbs', a complex configuration of the vacuolar membrane, is affected by mutations of vacuolar SNARE and phospholipase in *Arabidopsis.* Plant J. **68:** 64–73.

Saito, C., Uemura, T., Awai, C., Ueda, T., Abe, H., and Nakano, A. (2011b). Qualitative difference between "bulb" membranes and other vacuolar membranes. Plant Signal. Behav. **6:** 1914–1917.

Segami, S., Nakanishi, Y., Sato, M.H., and Maeshima, M. (2010). Quantification, organ-specific accumulation and intracellular localization of type II H^+-pyrophosphatase in *Arabidopsis thaliana.* Plant Cell Physiol. **51:** 1350–1360.

Shaner, N.C., Steinbach, P.A., and Tsien, R.Y. (2005). A guide to choosing fluorescent proteins. Nat. Methods **2:** 905–909.

Snapp, E.L., Hegde, R.S., Francolini, M., Lombardo, F., Colombo, S., Pedrazzini, E., Borgese, N., and Lippincott-Schwartz, J. (2003). Formation of stacked ER cisternae by low affinity protein interactions. J. Cell Biol. **163:** 257–269.

Sonnewald, U. (1992). Expression of *E. coli* inorganic pyrophosphatase in transgenic plants alters photoassimilate partitioning. Plant J. **2:** 571–581.

Subach, O.M., Malashkevich, V.N., Zencheck, W.D., Morozova, K.S., Piatkevich, K.D., Almo, S.C., and Verkhusha, V.V. (2010). Structural characterization of acylimine-containing blue and red chromophores in mTagBFP and TagRFP fluorescent proteins. Chem. Biol. **17:** 333–341.

Suga, S., Imagawa, S., and Maeshima, M. (2001). Specificity of the accumulation of mRNAs and proteins of the plasma membrane and tonoplast aquaporins in radish organs. Planta **212:** 294–304.

Suga, S., and Maeshima, M. (2004). Water channel activity of radish plasma membrane aquaporins heterologously expressed in yeast and their modification by site-directed mutagenesis. Plant Cell Physiol. **45:** 823–830.

Tamura, K., Shimada, T., Ono, E., Tanaka, Y., Nagatani, A., Higashi, S.I., Watanabe, M., Nishimura, M., and Hara-Nishimura, I. (2003). Why green fluorescent fusion proteins have not been observed in the vacuoles of higher plants. Plant J. **35:** 545–555.

Uemura, T., Yoshimura, S.H., Takeyasu, K., and Sato, M.H. (2002). Vacuolar membrane dynamics revealed by GFP-AtVam3 fusion protein. Genes Cells **7:** 743–753.

Uemura, T., Morita, M.T., Ebine, K., Okatani, Y., Yano, D., Saito, C., Ueda, T., and Nakano, A. (2010). Vacuolar/pre-vacuolar compartment Qa-SNAREs VAM3/SYP22 and PEP12/SYP21 have interchangeable functions in *Arabidopsis*. Plant J. **64:** 864–873.

Uversky, V.N., and Dunker, A.K. (2010). Understanding protein non-folding. Biochim. Biophys. Acta **1804:** 1231–1264.

van Putten, E.G., Akbulut, D., Bertolotti, J., Vos, W.L., Lagendijk, A., and Mosk, A.P. (2011). Scattering lens resolves sub-100 nm structures with visible light. Phys. Rev. Lett. **106:** 193905–193908.

Wang, L., Seeley, E.S., Wickner, W., and Merz, A.J. (2002). Vacuole fusion at a ring of vertex docking sites leaves membrane fragments within the organelle. Cell **108:** 357–369.

Yang, F., Moss, L.G., and Phillips, G.N., Jr. (1996). The molecular structure of green fluorescent protein. Nat. Biotechnol. **14:** 1246–1251.

Yang, H., Knapp, J., Koirala, P., Rajagopal, D., Peer, W.A., Silbart, L.K., Murphy, A., and Gaxiola, R.A. (2007). Enhanced phosphorus nutrition in monocots and dicots over-expressing a phosphorus-responsive type I H^+-pyrophosphatase. Plant Biotechnol. J. **5:** 735–745.

Yano, D., Sato, M., Saito, C., Sato, M.H., Morita, M.T., and Tasaka, M. (2003). A SNARE complex containing SGR3/AtVAM3 and ZIG/VTI11 in gravity-sensing cells is important for *Arabidopsis* shoot gravitropism. Proc. Natl. Acad. Sci. USA **100:** 8589–8594.

Zacharias, D.A., Violin, J.D., Newton, A.C., and Tsien, R.Y. (2002). Partitioning of lipid-modified monomeric GFPs into membrane microdomains of live cells. Science **296:** 913–916.